Fission dynamics of ^{240}Pu from saddle to scission and beyond

Aurel Bulgac,[1] Shi Jin,[1] Kenneth J. Roche,[2,1] Nicolas Schunck,[3] and Ionel Stetcu[4]
[1]*Department of Physics, University of Washington, Seattle, Washington 98195-1560, USA*
[2]*Pacific Northwest National Laboratory, Richland, Washington 99352, USA*
[3]*Nuclear and Chemical Science Division, Lawrence Livermore National Laboratory, Livermore, California 94551, USA*
[4]*Theoretical Division, Los Alamos National Laboratory, Los Alamos, New Mexico 87545, USA*

(Received 2 June 2018; revised manuscript received 25 June 2019; published 19 September 2019)

Calculations are presented for the time evolution of ^{240}Pu from the proximity of the outer saddle point until the fission fragments are well separated, using the time-dependent density functional theory extended to superfluid systems. We have tested three families of nuclear energy density functionals and found that all functionals exhibit a similar dynamics: The collective motion is highly dissipative and with little trace of inertial dynamics, due to the one-body dissipation mechanism alone. This finding justifies the validity of using the overdamped collective motion approach and to some extent the main assumptions in statistical models of fission. This conclusion is robust with respect to the nuclear energy density functional used. The configurations and interactions left out of the present theory framework only increase the role of the dissipative couplings. An unexpected finding is varying the pairing strength within a quite large range has only minor effects on the dynamics. We find notable differences in the excitation energy sharing between the fission fragments in the cases of spontaneous and induced fission. With increasing initial excitation energy of the fissioning nucleus, more excitation energy is deposited in the heavy fragment, in agreement with experimental data on average neutron multiplicities.

DOI: 10.1103/PhysRevC.100.034615

I. INTRODUCTION

Eighty years after the discovery of nuclear fission [1], a full microscopic description is still lacking, which in itself astonishing in quantum many-body theory. The term *nuclear fission* was coined by Meitner [2,3]. In 1934, Noddack [4] presented credible arguments that perhaps Fermi [5] had already created fission fragments in his laboratory. Fermi had bombarded uranium with neutrons but failed to observe the fission fragments by shielding his uranium target with a thin aluminum foil in order to minimize the background due to α particles [6], which likely blocked the fission fragments too [7]. Reasoning based on the Gamow theory of quantum tunneling led many at the time to expect that fission would occur on timescales many orders of magnitude longer than the age of the Universe. This explains the shock experienced by the scientific community when Hahn and Strassmann published their observations on January 6, 1939 (submitted on December 22, 1938, and unfortunately without Meitner as a coauthor) [1]. Meitner and Frisch [2], who became aware of these results during the last days of 1938, figured out the basic explanation of nuclear fission even before the Hahn and Strassmann paper appeared in print. They presented compelling arguments that Gamow's 1930 charged liquid drop model of nuclei [8,9], in which the Coulomb interaction between protons competes with the surface nuclear tension, leads to a very natural explanation of the main fission properties. The liquid drop model was almost immediately combined with Bohr's compound model and extended to deformed nuclei by Bohr and Wheeler [10]. According to Bohr and Wheeler [10], a low-energy incident neutron is captured by the uranium nucleus and leads to the formation of a compound nucleus [11]. For example, the energy levels in a compound nucleus are separated by $\Delta E \approx 10\,\text{eV}$ in the $^{232}\text{Th} + n$ reaction, and with similar order of magnitude in heavy nuclei [12–14]. Thus, the evolution of the nuclear shape from a rather compact one, corresponding to the ground state of uranium after the neutron capture until it reaches the fission barrier, lasts a relatively long time on the order $O(\frac{\hbar}{\Delta E}) = 0.6 \times 10^{-16}\,\text{s} = 2 \times 10^{7}\,\text{fm/c}$. This time is much longer than the time needed for a nucleon to traverse a nucleus back and forth, which is approximately $1.7 \times 10^{-22}\,\text{s} = 50\,\text{fm/c}$. As a result, the memory of the initial state is "forgotten" and statistical arguments can be use to describe the eventual decay of a compound nucleus and its decay various branching ratios [15,16]. The position of the fission barrier is determined by the nuclear elongation, where the rate of increase of the nuclear surface energy is exactly compensated by the rate of decrease of the Coulomb energy of the nucleus. Since the role of the shell effects and the formation of the fission isomer second well were understood only much later [17–19], Bohr and Wheeler could not tackle the asymmetric fission and theoretically addressed only the case of symmetric fission. After reaching the outer fission barrier, a nucleus evolves toward the scission configurations into two separated fission fragments (FFs) at a much faster rate. During this nonequilibrium evolution of the mother nucleus from saddle to scission, the properties of the FFs are defined.

Since an accurate solution of the time-dependent Schrödinger equation with realistic nucleon interactions will be out of reach for a very long time (if ever), the following question arises: What would be a reliable microscopic

approach? A Feyman's real-time path integral formulation [20,21] of quantum many-body systems is particularly appealing. The many-body wave function is represented as a sum over all possible paths joining the initial and final configurations, with appropriate weights:

$$\Psi(t) = \int \mathcal{D}[\sigma(t)] W[\sigma(t)] \exp\left(-\frac{i}{\hbar}\int_{t_i}^{t_f} \hat{h}[\sigma(t)]\right)\Psi(0), \tag{1}$$

where $\mathcal{D}[\sigma(t)]$ is an appropriate measure depending on all auxiliary fields, $W[\sigma(t)]$ is a Gaussian weight, and $\hat{h}[\sigma(t)]$ is a one-body Hamiltonian built with the auxiliary one-body fields $\sigma(t)$. $\Psi(0)$ is the initial wave function, often chosen as a (generalized) Slater determinant.[1]

Thus, the true many-nucleon wave function is now a time-dependent linear superposition of many time-dependent (generalized) Slater determinants. In this respect, the true many-nucleon wave function has a similar mathematical structure as the wave function in the time-dependent generator coordinate method (TDGCM) introduced by Wheeler *et al.* [22,23]; see Sec. II. One cannot fail but see here also the analogy in treating fluctuations around the mean-field trajectory with the classical Langevin description of nuclear collective motion as well [24]. The representation (1) (which is an exact one) of the many-body wave function has the great advantage that each trajectory is independent of all the others. In the stationary phase approximation, such a path integral selects a particular mean field, which can be interpreted as the most probable trajectory. This mean-field trajectory is not uniquely defined [20], and fluctuations around it are important. The current attitude in nuclear physics, even though usually not explicitly spelled out, is to simulate this particular path with a trajectory generated in time-dependent density functional theory (TDDFT).

Even though the mean paths along which nuclei evolve do not convey the whole story in fission, they do determine the most probable properties of this nonequilibrium quantum process. A complete microscopic characterization of the fission dynamics is still lacking, since practically all simulations performed so far have relied on a range of simplifying assumptions, the accuracy of which have not or could not have been tested. Here, we will consider only the most probable fission trajectories and leave the study of the role of fluctuations in a fully quantum mechanical formulation to future studies [25].

Many basic questions remained unanswered by the microscopic theory, and experiment provides often only indirect and hard-to-quantify insight. What is the nature of the driving force in fission dynamics? What is the mechanism that provides excitation energy to FFs at scission? How is this excitation energy between the FFs shared? Are the one-body [26] and/or the two-body excitation mechanisms effective? Are pairing correlations still important in the later stages of the evolution before scission? How many neutrons (if any) are emitted before and/or at scission and/or before the fission products are fully accelerated? Are ensembles of initial conditions important in modeling the FFs yields and properties? How does the initial excitation energy of the fissioning nucleus impact the excitation energy mechanism between FFs? How are the average neutron multiplicities as a function of the FF mass affected by the initial excitation energy of the fissioning system? The present study is our attempt to shed light on all these questions.

II. MAIN THEORETICAL APPROACHES TO FISSION DYNAMICS

The evolution of the nuclear shape from the ground state to the outer fission barrier is very slow and one often invokes the picture of an adiabatic evolution, particularly in the case of spontaneous fission. The description of the nuclear dynamics, starting when the nucleus exits or passes the outer fission barrier until it reaches the scission configuration, is treated in the literature either as an adiabatic evolution (leading to a conservative dynamics) or as a damped or even overdamped motion, using the same kind of parameters. There is no consensus in literature on the character of the dynamics during this last phase of fission, namely conservative or Hamiltonian versus dissipative dynamics or even overdamped motion. All different approaches, based on such different assumptions about the character of the fission dynamics, lead to reasonably accurate agreement with experimental results. So far, it has been impossible to observe directly in experiments this stage of the nuclear dynamics. Yet, the most important properties of the FFs, their masses and charges, their shapes and intrinsic excitation energies, are defined during this stage.

One class of microscopic theoretical models used to describe fission fragment yields is based on the time-dependent generator coordinate method (TDGCM) [22,23,27–33] or on the adiabatic time-dependent Hartree-Fock (ATDHF) theory [34–37]. It was established almost forty years ago that TDGCM with complex coordinates is basically equivalent to the ATDHF approach to large-amplitude collective motion (LACM) [38] and for that reason we will concentrate here on TDGCM alone. The wave function of a many-fermion

[1] In reality, the initial wave function is an ensemble of many Slater determinants, and while each member of the ensemble might break various symmetries, the total wave function satisfies all symmetries. Typically, a fissioning nucleus in its intrinsic ground state has a quadrupole deformation and positive parity, for example. However, on the way to the saddle, this state evolves into one with a non-vanishing octupole moment, which at first glance appears to be an impossible transition. In large many-body systems, however, one observes remnants of the spontaneous symmetry breaking, which strictly speaking exists only in infinite systems. The density of these states is, however, so large that the time for a nucleus to "tunnel" from one symmetry-breaking state to another, in order to restore the symmetry, is much larger that the time it takes a nucleus to evolve, for example, from a state with positive octupole momentum $Q_{30} > 0$ (in center-of-mass reference frame) to one with negative octupole momentum $Q_{30} < 0$, which in the long run will restore the parity. The large time difference in the scales of the processes which are responsible for the restoration of symmetries and the timescale of the fission dynamics in our case, allows us to focus on the dynamics of a single component of the ensemble at a time. We thank J. Randrup for urging us to shed light on this issue.

system in TDGCM is constructed according to the following prescription,

$$\Psi(\mathbf{x},t)=\int d\mathbf{q} f(\mathbf{q},t)\Phi(\mathbf{x}|\mathbf{q}), \tag{2}$$

where $\Phi(\mathbf{x}|\mathbf{q})$ are (generalized) Slater determinants depending on nucleon spatial coordinates, spin, and isospin $\mathbf{x}=(x_1,\ldots,x_A)$, $x_k=(\mathbf{r}_k,\sigma_k,\tau_k)$ and parameterized by the collective coordinates $\mathbf{q}=(q_1,\ldots,q_n)$ and where $f(\mathbf{q},t)$ is the collective wave function.

The collective coordinates can and are often interpreted as real degrees of freedom (DoF), which one assumes that can be decoupled from the rest, or the intrinsic DoF. The definition of collective and intrinsic DoF is still not a solved problem and it is not obvious even that a satisfactory solution even exists [39]. An alternative interpretation it to treat these "coordinates" as mere labels of the (generalized) Slater determinants. In that case, one can interpret $\mathbf{q}$ as labels of "sites" from to and where to the nucleus hops during evolution, a model which appears to be much simpler and almost as accurate as the GCM [40], in a manner analogous to the tight-binding models in condensed matter theory [41]. In the case when one takes at face value that $\mathbf{q}$ are real collective coordinates, the interpretation of the results in terms of "real collective" DoF could lead to inconsistencies of the emerging models and physical interpretation of the results. A particular source of difficulties lies in the fact that the total number of DoF in GCM $A+n$ is unphysical.

The representation (2) would be in principle exact if the (generalized) Slater determinants $\Phi(\mathbf{x}|\mathbf{q})$ would form a complete or overcomplete set. Even if this set is not complete but would be covering the phase space where the collective dynamics is concentrated, one would be able to derive accurate approximate representations in this manner. There are, however, reasons to believe that the set of (generalized) Slater determinants $\Phi(\mathbf{x}|\mathbf{q})$ used in the current implementation of TDGCM treatments is not sufficiently large in the case of fission dynamics; see Appendix C.

The equation for the collective wave function $f(\mathbf{q},t)$ is obtained from the Dirac variational principle for the wave function $\Psi(\mathbf{x},t)$ [by varying $f(\mathbf{q},t)$ with fixed $\Phi(\mathbf{x}|\mathbf{q})$]

$$\delta\int_{t_0}^{t_1}dt\int d\mathbf{x}\,\Psi^*(\mathbf{x},t)\left[i\hbar\frac{\partial}{\partial t}-H\right]\Psi(\mathbf{x},t)=0. \tag{3}$$

Under the Gaussian overlap approximation, the emerging integral equation for a related to $f(\mathbf{q},t)$ collective wave function $g(\mathbf{q},t)$ is transformed into a partial differential equation [27,28,30,32,37] similar to the equation of the Bohr-Mottelson Hamiltonian in the space of the collective degrees of freedom $\mathbf{q}$

$$i\hbar\frac{\partial g(\mathbf{q},t)}{\partial t}=\left[-\frac{1}{\sqrt{\gamma(\mathbf{q})}}\frac{\partial}{\partial q_k}\frac{\sqrt{\gamma(\mathbf{q})}\hbar^2}{2\mathcal{M}_{kl}(\mathbf{q})}\frac{\partial}{\partial q_l}+\mathcal{U}(\mathbf{q})\right]g(\mathbf{q},t), \tag{4}$$

with a collective inertia tensor $\mathcal{M}(\mathbf{q})$ and collective potential energy surface $\mathcal{U}(\mathbf{q})$. Here $\gamma(\mathbf{q})$ is the determinant of the metric in the collective space and we adopted the Einstein convention for summation over repeated indices. The collective potential energy is obtained by minimizing the energy for fixed values of the collective variables $\mathbf{q}$,

$$\mathcal{U}(\mathbf{q})=\langle\Phi_{\min}(\mathbf{q})|H|\Phi_{\min}(\mathbf{q})\rangle-\varepsilon_0(\mathbf{q}), \tag{5}$$

where $\Phi_{\min}(\mathbf{x}|\mathbf{q})$ is obtained by minimizing the functional $\mathcal{V}(\mathbf{q})$ with constraints and

$$\mathcal{V}(\mathbf{q})=\min_{\mathbf{x}}\langle\Phi_{\min}(\mathbf{q})|H-\sum_k\lambda_k Q_k|\Phi_{\min}(\mathbf{q})\rangle, \tag{6}$$

where Q_k are various constraints and the quantum average is over the intrinsic DoF $\mathbf{x}$. In the above formula for the collective potential energy, the last term is due to the zero-point energy fluctuations, which has to be included in actual calculations to avoid double counting. The total energy of the system is a sum of the collective kinetic energy and of the collective potential energy. Collective kinetic energy is due to the presence of collective flow in the dynamics but it also has a contribution due to the presence of zero-point fluctuations. The collective potential energy depends only on the spatial matter distribution but not on any collective currents. TDGCM or ATDHF microscopic approaches thus invoke the adiabaticity (no intrinsic entropy production) of the nuclear collective shape evolution, leading to no irreversible energy transfer from the small number of collective DoF to the large number of intrinsic DoF. The intrinsic system is always at zero temperature and entropy and all the kinetic energy is due to the collective DoF only. While evolving in the collective space, the nucleus is thus intrinsically always at zero temperature, as the local Fermi momentum distributions correspond to zero local temperature. If an energy transfer between collective $\mathbf{q}$ and intrinsic $\mathbf{x}$ DoF would be allowed, then at given values of the collective variables $\mathbf{q}$ reached during the actual dynamics

$$\langle\Phi(\mathbf{q})|H|\Phi(\mathbf{q})\rangle>\langle\Phi_{\min}(\mathbf{q})|H|\Phi_{\min}(\mathbf{q})\rangle, \tag{7}$$

and strictly speaking in such a case the collective motion is not conservative anymore and a collective potential energy does not exist. In Sec. V and Appendix C, we will expand on these aspects.

It is also natural to assimilate the collective dynamics with that of Brownian motion of the collective DoF in the bath of the intrinsic DoF [24] and describe the collective dynamics either with a classical Fokker-Planck equation or with an equivalent classical Langevin equation. Phenomenological classical Langevin description in nuclear physics is restricted in practice to a small space of collective variables ($\leqslant$5; e.g., elongation, mass asymmetry, neck size, and the two quadrupole deformations of the fragments) [42] and the number and the character of these collective DoF are not universally agreed upon. Such models require the evaluation of a potential energy surface, of a collective inertia tensor (in most approaches), of a dissipation tensor (for Langevin dynamics), and of a phenomenological temperature. When a collective Schrödinger equation is derived within the TDGCM or ATDHF for a subset of collective variables, the class of quantum fluctuations generated is different from the thermal fluctuations generated in Langevin approaches [24,43–48]. However, TDGCM, ATDHF, and most incarnations of the Langevin approach rely on the assumption that the shape evolution is mostly collective in nature and driven both by

the potential energy surface and the inertia tensor. We provide here evidence that this assumption is invalid.

In experiments, the observed final state of nuclear fission corresponds to a wide FFs distribution of varying charges and masses and a wide distribution of their kinetic and excitation energies, angular momenta, and parities. Various Langevin implementations and TDGCM approaches suggest that the fluctuations around the most probable trajectory determine the distributions of the FFs on mass, charge, kinetic, and excitation energies. Accounting for fluctuations is also important quantum mechanically for totally different and unrelated reasons, to restore spontaneously broken symmetries. As Langevin-type simulations and the path-integral formulation both demonstrate, the presence of fluctuations along the entire trajectory is crucial, and the presence of initial-state fluctuations alone is of little consequence. We will demonstrate that since the nuclear collective dynamics from saddle to scission is similar to that of a very viscous fluid, the role of fluctuations only at the start of trajectories is quickly erased, and thus in total disagreement with the results of Ref. [49]; see also Appendix E.

In statistical scission-point models, there is no dynamics and only the competition between FFs configurations at the scission point are considered [50–52], a model to which our results lend partial support. In a statistical scission-point model, a full thermalization of the intrinsic DoF is implied. However, it is not obvious that all possible equilibrated configurations can be reached dynamically during the evolution from saddle to scission. On the other hand, our results lend some theoretical support to the overdamped Brownian motion model of Randrup *et al.* [43,44,53–55].

III. THEORETICAL FRAMEWORK

Our theoretical framework is called the time-dependent superfluid local density approximation (TDSLDA), which is an extension of TDDFT to superfluid systems [56–58]. DFT, which formally looks similar to the Hartree approximation, is used in the Kohn-Sham implementation, often referred particularly in condensed matter and chemistry literature as local density approximation (LDA). As a natural extension of Kohn-Sham LDA, SLDA stands the superfluid LDA. SLDA equations formally appear as local Hartree-Fock-Bogoliubov (HFB) or Bogoliubov–de Gennes equations. The equations for the single-particle (sp) wave functions are not obtained from the expectation of a Hamiltonian with interparticle interactions using (generalized) Slater determinants but from an energy density functional, which in accordance with the DFT philosophy should include all possible correlations.

Within TDSLDA, the evolution of the quasiparticle wave functions (qpwfs) is governed by the equations:

$$i\hbar\frac{\partial}{\partial t}\begin{pmatrix} u_{k\uparrow} \\ u_{k\downarrow} \\ v_{k\uparrow} \\ v_{k\downarrow} \end{pmatrix} = \begin{pmatrix} h_{\uparrow\uparrow} & h_{\uparrow\downarrow} & 0 & \Delta \\ h_{\downarrow\uparrow} & h_{\downarrow\downarrow} & -\Delta & 0 \\ 0 & -\Delta^* & -h^*_{\uparrow\uparrow} & -h^*_{\uparrow\downarrow} \\ \Delta^* & 0 & -h^*_{\downarrow\uparrow} & -h^*_{\downarrow\downarrow} \end{pmatrix} \begin{pmatrix} u_{k\uparrow} \\ u_{k\downarrow} \\ v_{k\uparrow} \\ v_{k\downarrow} \end{pmatrix}, \tag{8}$$

where we have suppressed the spatial $\boldsymbol{r}$ and time coordinate t, and k labels the qpwfs (including the isospin) $[u_{k\sigma}(\boldsymbol{r},t), v_{k\sigma}(\boldsymbol{r},t)]$, with $\sigma = \uparrow, \downarrow$ the z projection of the nucleon spin. The sp Hamiltonian $h_{\sigma\sigma'}(\boldsymbol{r},t)$ and the pairing field $\Delta(\boldsymbol{r},t)$ are functionals of various neutron and proton densities, which are computed from the qpwfs; see Ref. [59] for technical details. No proton-neutron pairing is assumed in the present study, and the pairing field is singlet in character. A TDSLDA extension to a more complex pairing mechanism is straightforward.

A definite advantage of the TDSLDA approach is the size of the quasiparticle space. In any numerical solution of quantum mechanical equations, the relevant question is how many "basis states" one should include in the analysis in order to ensure a physically correct description of the dynamics. In a dynamical study of fission, one places the nucleus on a spatial rectangular lattice. One needs a simulation box spatially large enough to accommodate both the mother and the receding FFs until they do not significantly influence each other. At the same time, the single-particle momenta allowed should be high enough to faithfully describe the single-particle dynamics. The number of needed "basis states" can then estimated from a simple formula (see Ref. [60] and also Appendix A for further details):

$$\mathcal{N}_{\rm sp} = 2 \times \frac{L_x L_y L_z \times (2p_c)^3}{(2\pi\hbar)^3} = 2N_xN_yN_z, \tag{9}$$

$$L_{x,y,z} = N_{x,y,z}\, l, \quad p_c = \frac{\pi\hbar}{l}, \tag{10}$$

where the factor 2 accounts for the spin, $L_{x,y,z} = N_{x,y,z}l$ are the side lengths of the spatial simulation box, $N_{x,y,z}$ are the number of lattice points in each spatial direction, l is the lattice constant, and p_c is the single-particle momentum cutoff. In Fig. 1, we illustrate the difference between the size of the Hilbert space in a dynamical calculation and the size of the Hilbert space used in a configuration space approach [61] of stationary states. (The size of the quasiparticle Hamiltonian for either neutrons or protons is $4N_xN_yN_z$ when placed on a spatial lattice.) Most of the quasiparticle states are initially unoccupied, but during the dynamics single-particle levels move up and down and mix, see Fig. 3, and initially unoccupied high-lying states are occupied.

In our proof-of-concept study [62], we chose rather arbitrarily to use the SLy4 nuclear energy density functional (NEDF) [63], which accurately describes a large body of nuclear observables throughout the nuclear mass table, even though this functional is not particularly popular among fission practitioners. So far there is no deep understanding of why the properties of various NEDFs used for fission calculations are responsible for the agreement or the disagreement with observations. However, as Meitner and Frisch [2] and subsequent studies have shown, only a small number of basic nuclear properties (nuclear incompressibility, surface tension, and Coulomb interaction) were need to understand the qualitative and to some extent the quantitative features (notably, the energy released in fission) of nuclear fission. Accounting for spin-orbit interaction and pairing correlations [17–19] was sufficient to further explain many of the remaining

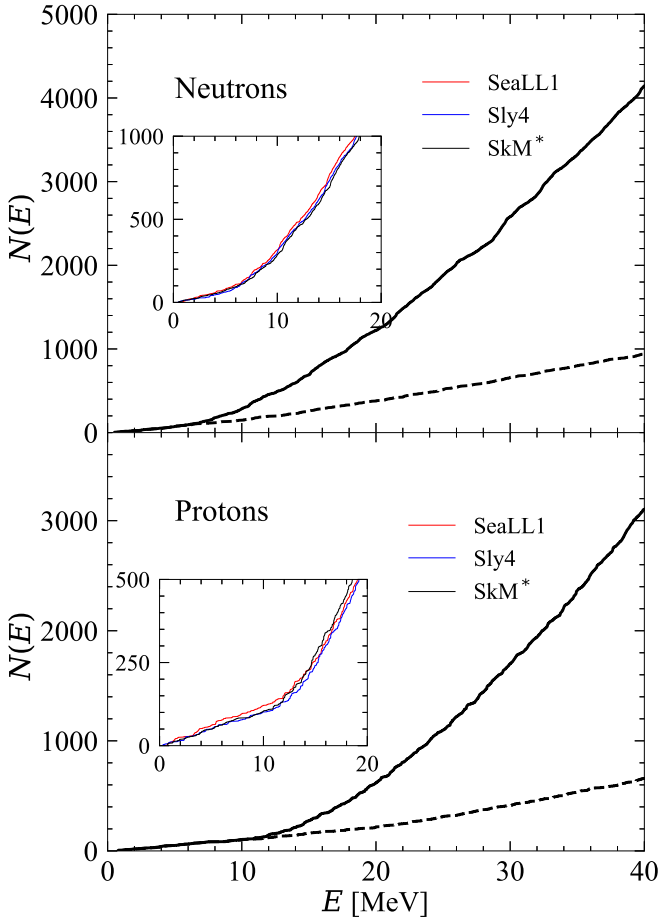

FIG. 1. The cumulative number of quasiparticle states for neutrons and protons obtained in a full diagonalization of the (initial) stationary quasiparticle Hamiltonian with constraints [see Eq. (A6)] for neutrons and protons in a discrete variable representation used in (TD)SLDA (solid line) and using the configuration space approach [61] (dashed line) in case of SkM* NEDF. The insets show the cumulative number of quasiparticle energies for SeaLL1 (red), SLy4 (blue), and SkM* (black) NEDFs respectively. The maximum quasiparticle energy is ≈400 MeV in (TD)SLDA while in HFBTHO is ≈100 MeV. The total number of quasiparticle states, for either neutrons or protons, is $2N_xN_yN_z = 2 \times 24^2 \times 48 = 55\,296$ in the present numerical implementation. In SLDA, the single-particle level density increases sharply above the nucleon separation energy, as physically expected. As a result, above the nucleon separation energy the configuration space approach severely underestimates the single-particle level density.

properties of the fission dynamics, e.g., asymmetric fission, odd-even staggering effects, etc. Many other details of the several hundreds of existing NEDFs differ often greatly but never lead to significant improvements over treatments based only on describing the basic nuclear properties enumerated above [42,64–67].

Hundreds of NEDFs have been introduced [68], depending on a large number of parameters, and the fitting criteria used are not universally established. SkM* [69] and UNEDF1 [70] NEDFs have been designed to accurately describe fission properties and the profiles of the corresponding potential

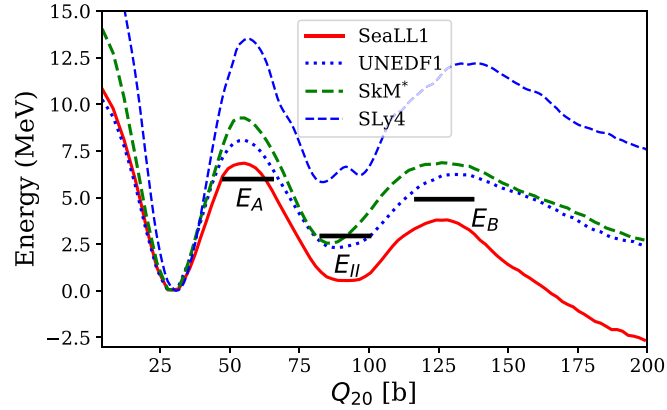

FIG. 2. Fission pathway for ^{240}Pu along the mass quadrupole moment Q_{20} calculated with SeaLL1, SkM*, and UNEDF1. With black horizontal lines labeled by E_A, E_B, and E_{II}, we show the values of the inner and outer fission barriers and the energy of the fission isomer with respect to the ground-state energy.

energy surface are very similar. We have adopted SkM* in this study. The other NEDF we chose is the recently developed SeaLL1 [71], which unlike the hundreds of NEDFs introduced in the literature, relies on the smallest number of fitting parameters, all of them tied to basic nuclear properties, and delivers one of the best global descriptions of a large number of nuclear properties (masses, charge radii, compressibility, surface tension, isospin symmetry, shell structure, pairing, two-nucleon separation energies, etc.). In Fig. 2, we compare the profiles of the fission pathways for SLy4, SeaLL1, UNEDF1, and SkM*. These calculations were performed with the HFBTHO density functional theory (DFT) solver [61], triaxiality is not included, and the height of the first fission barrier is typically overestimated for these functionals by about 2 MeV or even more in case of SLy4 [72]. Compared with SkM* and UNEDF1, SeaLL1 underestimates the excitation energy of the fission isomer ($E_{II} = 0.54$ MeV compared with an experimentally extracted value of 2.8 MeV) and the heights of the extracted fission barriers ($E_A = 6.84$ MeV vs 6.05 MeV and $E_B = 4.20$ MeV vs 5.15 MeV, respectively, for the inner and outer barriers) agree within 1 MeV.

Both SkM* and UNEDF1 were constrained specifically on the height of the first fission barrier (SkM*) or excitation energy of the fission isomer (UNEDF1), while no specific information for nuclei at large deformation in constructing SeaLL1 was used. Without any such constraint, the resulting NEDF is still in reasonable agreement with experimental results, especially the height of the two barriers. Our results are definitely better than predictions with SLy4 [63], which predicts the second fission barrier higher than the first one, after one includes beyond-mean-field corrections [73]. The differences between the extracted and calculated fission barriers with NEDF designed for fission can reach 2.5 MeV, see Ref. [74], where fission barriers and the energy of the second isomer in chains of Ra, Th, U, Pu, Cm, and Cf are compared to the UNEDF1-2, Gogny D1S [75], and FRLDM [66] functionals. In a recent study of the surface energy coefficient for 76 parametrizations of the Skyrme NEDF [76], it was

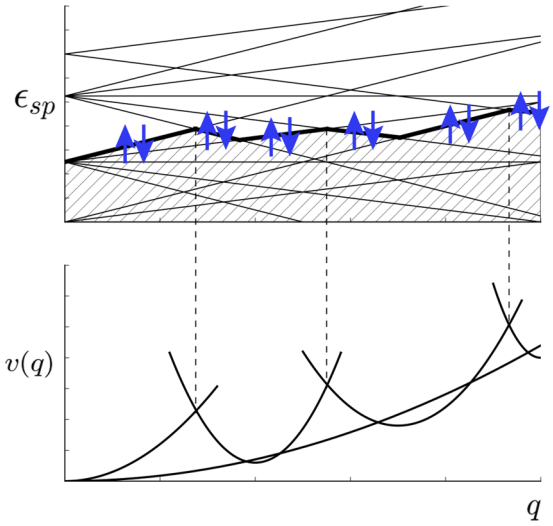

FIG. 3. Schematic evolution of sp levels of nucleons (upper panel) and the total nuclear energy (lower panel) as a function of deformation parameter q [77,78]. The thick line represents the Fermi level and the up and down arrows depict the Cooper pairs of nucleons on the Fermi level only, in time-reversed orbits $(m, -m)$.

shown that the energy of the fission isomer and the height of the outer fission barrier vary by several MeVs with respect to the ground-state energy.

Apart from exploring the sensitivity of fission dynamics characteristics on the NEDF properties, it is also imperative to study the sensitivity of TDDFT trajectories with respect to their initial conditions. Bohr's compound nucleus model [11] would suggest that initial conditions in general should not matter. Initial conditions near the outer fission barrier might matter, however, as the dynamics from the outer fission barrier onward is faster than starting from the ground-state configuration after capturing a neutron. On the other hand, Feyman's path-integral approach and the phenomenological Langevin approach, see Sec. I, would suggest that fluctuations along the fission path, not initial fluctuations, should dominate the dynamics. Recently, a claim was made that fluctuations in an ensemble of peculiarly chosen initial conditions alone with absolutely no fluctuations along the fission path would be sufficient in order to describe the FFs yields and the total kinetic energy (TKE) distributions [49], a claim which our results conspicuously do not support.

IV. ROLE OF PAIRING CORRELATIONS

The essential role of pairing correlations in nuclear shape dynamics has been addressed qualitatively in the past. A simplified picture was presented by Hill and Wheeler [22] and was later refined by Bertsch [77–80], who emphasized the crucial role played by the pairing interaction. While a nucleus deforms, the sp levels move up and down, and typically cross in the absence of pairing, as shown in Fig. 3. The sp occupation probabilities remain unchanged if levels cross, which in the case of large prolate shapes leads to a very oblate Fermi surface and thus to a volume energy excitation of the nucleus. As Meitner and Frisch [2] have correctly assumed, during fission the nuclear volume practically does not change and only the surface area increases. Thus, a volume type of energy excitation is excluded. As sp levels are doubly occupied due to Kramers degeneracies, only the pairing short-range interaction can provide a very effective mechanism to move simultaneously a pair of nucleons in time-reversed states from one level to another at an (avoided) crossing [77–80]. The probability of such transitions is particularly enhanced in the presence of a Bose-Einstein condensate of Cooper pairs, but such transitions remain important even in the absence of the condensate.

Apart from the arguments that the nuclear volume does not change and therefore the local Fermi sphere should remain spherical, the fact that fission is hindered in the absence of pairing correlations (at least at the mean field level) was demonstrated recently in Refs. [81–83].

To illustrate the crucial role played by the pairing correlations in fission dynamics, we performed a TDSLDA simulation with an initial configuration identical to the S3 case of Ref. [62], but enforcing stronger pairing correlations by increasing the absolute value of bare coupling constant g_0. The corresponding average neutron and proton pairing gaps in the initial state increase from 0.73 and 0.33 MeV to 2.57 and 1.62 MeV, respectively. By increasing the strength of the pairing field, the fission dynamics proceeds approximately 10 times faster. Figure 4 shows the snapshots of the number density, magnitude of pairing field, and phase of pairing fields for neutron and proton, respectively, in these two simulations. The left three columns in Fig. 4 show the induced fission of ^{240}Pu with realistic pairing strength, which lasts up to 14 000 fm/c from saddle to scission, while the right three columns show the dynamics with an enhanced pairing strength, which lasts only about 1 400 fm/c. In the case with normal pairing strength, the pairing field on the way from saddle to scission fluctuates noticeably in magnitude and phase. Therefore, strictly speaking, the pairing field during its time evolution stops being a superfluid condensate of Cooper pairs, which otherwise would exhibit a long-range order. However, in the case with larger pairing strength, the pairing field shows the expected characteristics of a slowly evolving superfluid condensate, the nuclear fluid behaving almost like a perfect or ideal fluid. This pattern was also observed in case of collision of two superfluid heavy ions [84,85]. Even though realistic pairing correlations are relatively weak, they still provide the essential "lubricant" for the saddle-to-scission evolution to take place.

V. RESULTS

We have chosen an ensemble of initial conditions in the Q_{20}, Q_{30} collective coordinates, in total 60 different initial conditions (including the four trajectories from Ref. [62]), as shown in Fig. 5. These initial conditions are prepared by constrained HFB calculations with the HFBTHO solver [61]. Using these densities, we generated the raw qpwfs used as initial conditions in the time-dependent simulations, in the absence of any constraints; see Appendix A for details.

One set of initial conditions (SeaLL1-1) corresponds to configurations of ^{240}Pu with mean excitation energy and

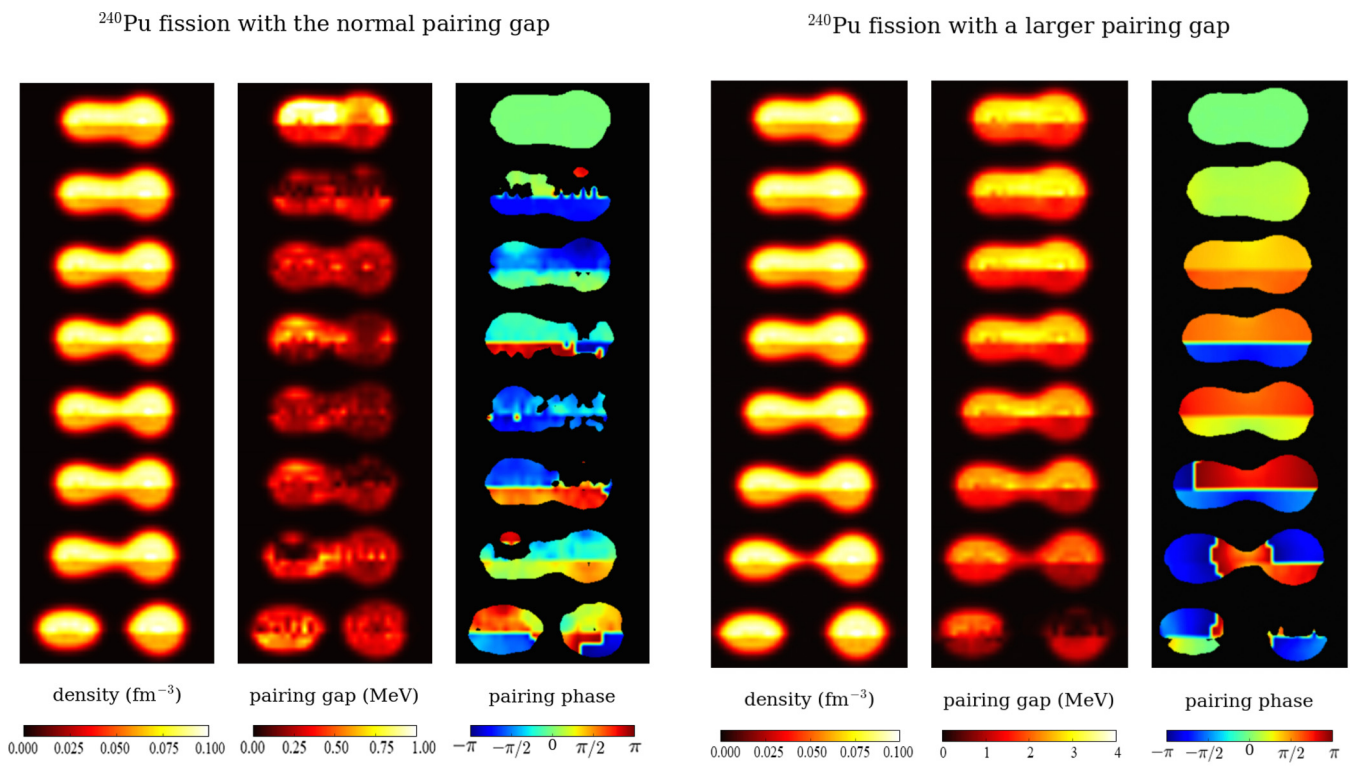

FIG. 4. The left three columns shows the induced fission of ^{240}Pu with normal pairing strength, which lasts up to 14 000 fm/c ($\approx 47 \times 10^{-21}$ s) from saddle to scission. The columns show sequential frames of the density (first column), the magnitude of the pairing field (second column), and the phase of the corresponding pairing field (third column). The upper and lower parts of each frame show the neutron and proton densities, the magnitudes of neutron and proton pairing fields, and the phase of the pairing field, respectively [62]. The right three columns show the corresponding snapshots of the induced fission of ^{240}Pu with enhanced pairing strength, which lasts about 1 400 fm/c.

variance of 7.9 and 1.7 MeV in the neighborhood of the outer saddle point, which can be reached in low-energy neutron induced fission. The other set of initial conditions (SeaLL1-2) corresponds to a mean excitation energy and variance of 2.6 and 1.8 MeV, which can be reached either in spontaneous fission or with photoexcitation excitation of ^{240}Pu. The third set of initial conditions (SkM*-1) is similar to SeaLL1-1, with mean excitation energy and variance of 8.2 and 3.0 MeV, but with an increased pairing strength. The fourth set (SkM*-2) was characterized by a realistic pairing strength. In the simulations with SLy4 NEDF [63] and SkM*, we neglected the correction term $1/A$ for the center-of-mass kinetic energy in the sp kinetic energy $1 - 1/A$. Without this correction term, these NEDFs satisfy local Galilean invariance. We have checked that this term has a negligible influence on the profile of the potential energy surface.

A. Fission fragments properties

The most surprising outcome of these simulations is that in all these sets of initial conditions, which correspond to vastly different initial values of Q_{20}, Q_{30}, we observed a very strong focusing effect and the final states are remarkably similar; see Fig. 5. The heavy fragments have neutron and proton numbers between those of the double magic ^{132}Sn ($N = 82, Z = 50$) and of the octupole shaped ^{144}Ba ($Z = 56, N = 88$), and has a shape quite close to spherical. The lighter fragment has an elongated shape (see also Table II). Simenel and Scamps [86] have recently shown that the octupole shell stabilization of nuclei close to ^{144}Ba with $Z = 56$ drive the fission dynamics toward proton numbers larger than 50, as we also appear to confirm. As we show below, see Sec. V D and Fig. 10, at scission both FFs have a significant octupole deformation, which, however, relaxes after the FFs separate. The neutron and proton numbers (and thus the mass) of the FFs match pretty well to the mean values of the experimental systematics but show a very small dispersion; see Table I.

The strong focusing effect we have establish in the present study is in stark contrast with the results of Tanimura *et al.* [49]. The authors of that study generated an ensemble of initial conditions according to the stochastic mean field model of Ayik [87]. In the stochastic mean-field model, the nucleon single-particle wave functions (spwfs) are evolved using the old-fashion TDHF method and the only difference is in considering an ensemble of different initial conditions for the one-body density matrix [49,87] and Appendix E, which result in an ensemble of initial states with different initial energies and quadrupole Q_{20} and octupole Q_{30} moments. In this respect, our choice of various initial conditions spread over a significant area of the potential energy surface, the choice chosen by Tanimura *et al.* [49], and the subsequent time-dependent evolution of the nucleonic spwfs are qualitatively similar but the final results are qualitatively different. We attribute these differences to the fact that the

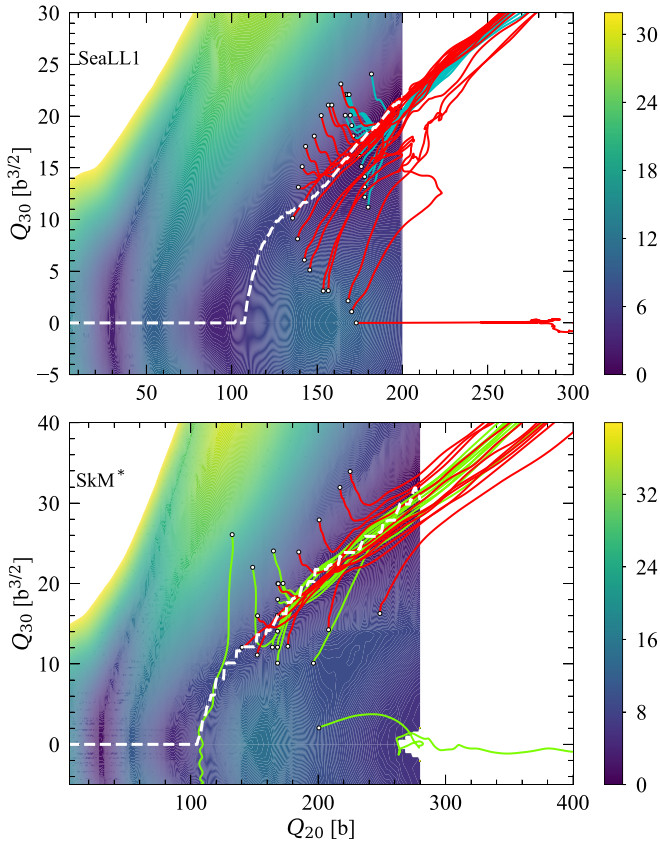

FIG. 5. Fission trajectories for SeaLL1 (upper panel) and SkM* (lower pannel). The red (SeaLL1-1) and cyan lines (SeaLL1-2) correspond to initial configurations slightly above and below the outer fission barrier. The SeaLL1-1sy trajectory had a small initial left-right asymmetry. The green lines in the lower panel correspond to SKM*-1asy and and the red lines to the trajectories obtained with SkM*-2asy. The white dashed lines show the path linking the ground-state minimum, the fission isomer minimum, and the inner and the outer saddle points. In both panels, we also show an example of a symmetric fission trajectory and in the low panel also of a trajectory which wondered inside the fission isomer well.

stochastic mean-field approach leads to flagrant violations of the Pauli principle; see Appendix D.

The TKE and total excitation energy (TXE) are also calculated. The TKE at a relatively large finite separation between the fragments (≈25 fm) and in the center-of-mass reference frame is evaluated with the formula

$$E_{\rm TKE} = \tfrac{1}{2}mA_{\rm H}\vec{v}_{\rm H}^2 + \tfrac{1}{2}mA_{\rm L}\vec{v}_{\rm L}^2 + E_{\rm Coul}, \tag{11a}$$

with the velocity of the fragment $f = H, L$ given by

$$\vec{v}_f = \frac{1}{mA_f}\int_{V_f} d\mathbf{r}\vec{j}(\boldsymbol{r}), \quad A_f = \int_{V_f} d\mathbf{r}n(\boldsymbol{r}), \tag{11b}$$

where $\vec{j}(\boldsymbol{r})$ and $n(\boldsymbol{r})$ are the total current and number densities respectively, and the integral is performed over the appropriate half-box V_f where each fragment is located. The Coulomb interaction energy (direct term only) is given by

$$E_{\rm Coul} = e^2\int_{V_{\rm H}} d\mathbf{r}_1\int_{V_{\rm L}} d\mathbf{r}_2\frac{n_p(\boldsymbol{r}_1)n_p(\boldsymbol{r}_2)}{|\boldsymbol{r}_1-\boldsymbol{r}_2|}, \tag{11c}$$

where $n_p(\boldsymbol{r})$ is the proton number density.

The excitation energy of each FF is calculated by extracting the computed ground-state energy of each FF from the energy of each FF in its rest frame. The FF ground-state energy is computed with the HFBTHO code [61] for the corresponding FF neutron and proton numbers. The proton and neutron numbers of FFs are evaluated from

$$Z_f = \int_{V_f} d\mathbf{r}n_p(\mathbf{r}), \quad N_f = \int_{V_f} d\mathbf{r}n_n(\mathbf{r}), \tag{12}$$

and the TXE is evaluated from

$$E_{\rm TXE} = E_{\rm H}^* + E_{\rm L}^*. \tag{13}$$

The energy variance of the TKE and TXE are only slightly larger than those of the initial energies. Compared to SeaLL1-2, the SeaLL1-1 starts at a larger excitation, and it has a longer average saddle-to-scission time ($\tau_{s\to s}$) and larger average TXE for the fission fragments, while their average TKEs are almost the same. When comparing the FFs characteristics emerging from simulations with SeaLL1 in Fig. 4 (see also Sec. IV), we notice that in the case of enhanced pairing the scission configuration corresponds to a longer neck and thus to a lower TKE. This is also confirmed by the results obtained with NEDF SkM*-1 (enhanced pairing strength) and SkM*-2 (realistic pairing strength). Another particular aspect that emerges from our simulations is the character of the excitation energy sharing between the light and heavy fragments. In the case of SeaLL1-1, the light fragment has a larger excitation

TABLE I. The NEDF, the initial excitation energy $E^*_{\rm ini}$, TKE, neutron, proton number, excitation energies of the heavy and light fragments, total excitation energy of fragments TXE, the sum of TKE and TXE, the average saddle-to-scission times, and their corresponding variances in parentheses. All energies are in MeV and S***sy, S***asy stand for symmetric and antisymmetric channels. Using Wahl's charge systematics [90] and data from Ref. [91], one obtains for neutrons $N_L^{\rm syst} \approx 61$ and $N_H^{\rm syst} \approx 85$ and for protons $Z_L^{\rm syst} \approx 40$ and $Z_H^{\rm syst} \approx 54$, and $\rm TKE^{syst} = 177\ldots178$ MeV from Ref. [92].

NEDF	$E^*_{\rm ini}$	TKE	$N_{\rm H}$	$Z_{\rm H}$	$N_{\rm L}$	$Z_{\rm L}$	$E^*_{\rm H}$	$E^*_{\rm L}$	TXE	TKE+TXE	$\tau_{s\to s}$ (fm/c)
SeaLL1-1asy	7.9(1.7)	177.8(3.1)	83.4(0.4)	53.2(0.4)	62.9(0.5)	41.1(0.4)	17.1(3.0)	20.3(2.0)	37.4(3.1)	215.2(2.5)	2317(781)
SeaLL1-2asy	2.6(1.8)	178.0(2.3)	82.9(0.4)	52.9(0.2)	63.3(0.5)	41.5(0.3)	19.5(3.8)	14.0(1.9)	33.5(5.1)	211.5(3.3)	1460(176)
SeaLL1-sy	9.2	147.1	77.5	48.9	68.8	45.4	45.2	29.0	74.2	221.3	10103
SkM*-1asy	8.2(3.0)	174.5(2.5)	84.1(0.9)	53.0(0.5)	61.8(0.9)	40.9(0.5)	16.6(3.1)	14.9(2.3)	31.5(3.8)	206.0(2.4)	1214(448)
SkM*-1sy	9.6	149.0	73.4	47.2	72.6	46.7	29.4	28.5	57.9	206.9	3673
SkM*-2asy	8.1(0.2)	182.8(4.4)	82.6(1.0)	52.4(0.6)	63.6(1.0)	41.7(0.5)	14.3(3.9)	13.0(3.0)	27.3(3.4)	210.1(1.8)	1349(309)

TABLE II. Internal temperatures for the light $T_{\rm L}$ and heavy $T_{\rm H}$ fragments computed according to the simple estimate (columns 2 and 3) or finite-temperature HFB calculations (columns 4 and 5). The axial quadrupole and octupole moments of the fragments, the ratios of the long to the short semiaxes, and the average scission times are also listed

NEDF	$T_{\rm L}$ [MeV]	$T_{\rm H}$ [MeV]	$T_{\rm L}$ [MeV]	$T_{\rm H}$ [MeV]	$Q_{20}^{\rm L}$ [b]	$Q_{20}^{\rm H}$ [b]	$Q_{30}^{\rm L}$ [b$^{3/2}$]	$Q_{30}^{\rm H}$ [b$^{3/2}$]	$(c/a)_H$	$(c/a)_L$	$\tau_{s\to s}$ [fm/c]
SeaLL1-1	1.40(0.07)	1.11(0.08)	1.28(0.07)	1.16(0.07)	15.7(0.9)	2.6(0.5)	0.08(0.17)	−0.20(0.06)	1.06(0.01)	1.59(0.03)	2392(800)
SeaLL1-2	1.15(0.08)	1.19(0.12)	1.00(0.08)	1.21(0.08)	17.1(1.1)	2.6(0.6)	0.23(0.08)	−0.19(0.06)	1.06(0.01)	1.63(0.03)	1460(176)
SeaLL1-sy	1.54	1.99			27.4	27.0	0.9	−1.1	1.87	1.73	10103
SkM*-1asy	1.20(0.09)	1.10(0.10)			11.3(1.3)	3.5(0.9)	0.1(0.1)	−0.4(0.1)	1.08(0.02)	1.42(0.04)	1214(448)
SkM*-1sy	1.56	1.55			24.2	25.6	0.9	−1.0	1.72	1.75	3673
SkM*-2asy	1.11(0.14)	1.02(0.14)			14.5(1.7)	2.3(0.7)	0.09(0.08)	−0.3(0.1)	1.05(0.02)	1.53(0.06)	1349(309)

energy than the heavy fragment, while the case of SeaLL1-2 has the opposite pattern. These differences lead us to conclude that the excitation energy sharing in the cases of spontaneous fission and induced fission are different. The observed wider mass yields for ^{239}Pu(n, f) than in ^{240}Pu (s.f.) [88,89] apparently point to differences in the over the barrier and under the barrier fission dynamics too.

It is instructive to express excitation energy of the FFs in terms of an internal temperature. We have used two different methods to extract this temperature. In the first approach, we have estimated the temperatures of the light and heavy fragments by the simple formula $E_f^* = \frac{A_f T_f^2}{a}$, where T_f is its temperature and $a \approx 10$ [12]. Such simple estimates are often used in simulations of the decay of the fission fragments using either Hauser-Fesbach or statistical evaporation models [93–96].

In the second approach used to determine the FFs temperatures, we have performed full finite-temperature HFB calculations with the HFBTHO solver. Calculations were performed by constraining N_f, Z_f, $\langle \hat{Q}_{20}^f \rangle$, and $\langle \hat{Q}_{30}^f \rangle$ to the values extracted in the relaxed fragments; see Tables I and II and Sec. V D. For each individual FF, we extract the temperature from the function $E_f^*(T)$ and find the corresponding T_f for the given E_f^*. This calculation is more realistic than the simple estimate, even though (i) by constraining only $\langle \hat{Q}_{20} \rangle$ and $\langle \hat{Q}_{30} \rangle$, we do not obtain exactly the same shape as the actual FFs and (ii) the temperature thus obtained should be thought of as the maximum allowable value; see discussion in Ref. [97]. In Table II, columns 2 and 3 list the average and variance over various trajectories of the temperature of light and heavy fragments in the first approach and columns 4 and 5 list the values in the second approach. These two approaches give comparable results and while in SeaLL1-1 the light fragments have higher temperature than the heavy fragments, in SeaLL1-2 the opposite is true. The relaxed values of the average and of the variance over the ensemble of trajectories of the quadrupole and of the octupole moments of fragments, see Fig. 10 and Section V D, are listed in columns 6 to 9. In columns 10 and 11, the ratio of the long to the short semiaxes of relaxed FFs are listed. As the initial-state excitation energy increases, from SeaLL1-2 to SeaLL1-1, one notices that the extra energy mostly goes to the light FF. This suggests that the average neutron multiplicity spectrum of spontaneous and neutron-induced fission could be noticeably different.

The total energy released $Q = E_{\rm TKE} + E_{\rm TXE}$ can be estimated alternatively with known FFs neutron and proton numbers, cf. Table I, by using a liquid drop model mass formula for the masses of the mother and daughter nuclei, including also the initial excitation energy. Using the the liquid drop mass parameters $a_v = -15.47$ MeV, $a_s = 16.73$ MeV, $a_I = 22.87$ MeV, and $a_c = 0.699$ MeV,

$$E_{gs} = a_v A + a_s A^{2/3} + a_I \frac{(N-Z)^2}{A} + a_c \frac{Z^2}{A^{1/3}}, \qquad (14)$$

obtained in Ref. [71] by fitting 2375 measured nuclear masses [98] with an energy rms 3.30 MeV, one obtains for SkM*-2asy trajectories $Q = 205$ MeV, as compared to 210.1 MeV from the simulation; see Table I. With the parameters $a_v = -15.77$ MeV, $a_s = 17.50$ MeV, $a_I = 23.65$ MeV, and $a_c = 0.723$ MeV obtained by fitting the ground-state masses evaluated with SeaLL1 in Ref. [71], we obtain 215.0 MeV for SeaLL1-1asy and 210.9 MeV for the SeaLL1-2ays, as compared to the calculated mean values 215.2 MeV and 211.5 MeV respectively; see Table I. This last (unoptimized) parametrization of the liquid drop mass formula reproduces the SeaLL1 ground-state energies in mean field (without beyond-mean-field corrections) for 606 even-even nuclei with mean energy error of 0.97 MeV and an energy rms of 1.46 MeV.

From the ensemble of initial conditions used to generate the fission trajectories in the case of NEDF SeaLL1, which have a significant spread in initial energies and the corresponding FFs excitation energies, we determined the average ratio of the temperatures $R_T = T_L/T_H$ as a function of the equivalent incident neutron energy E_n in the reaction ^{239}Pu(n, f), using for each FF the simple estimate $E_f^* = \frac{A_f T_f^2}{a}$. We parametrize the energy dependence obtained in the calculations by approximating R_T^2 with a linear function of E_n (while we do not expect an overall linear dependence, this should be a good approximation for up to about 5.5-MeV incident neutron energies). This linear dependence is added as a multiplicative factor, $R_T(A, E) \approx R_T(A) f(E_n)$, to the parameterization of the energy sharing in the Cascade Gamma Multiplicity for Fission (CGMF) code, which is used to model the neutron and γ emission [93,94,103]. Experimental evidence for the energy sharing is indirectly provided by detecting the average number of fission neutrons emitted as a function of fragment mass. In CGMF, the default calculation parameterizes this sharing by assuming a mass dependence

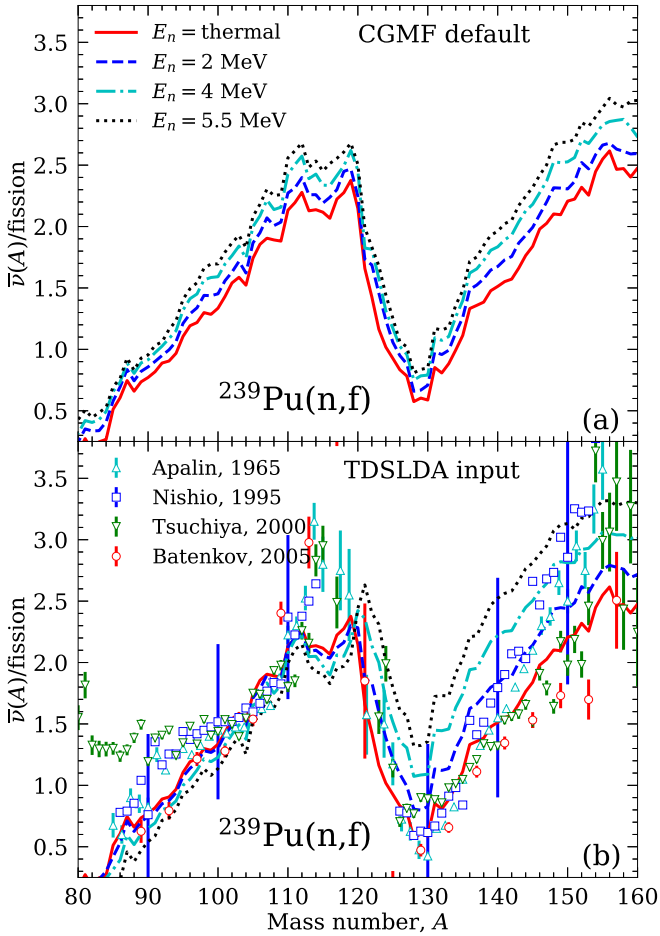

FIG. 6. We compare here the average neutron multiplicity $\bar{\nu}(A)$ emitted by FFs in the case of a default CGMF simulation, which assumes no E_n dependence for the energy sharing, with the one extracted using the the excitation energy sharing between the FFs in our calculation with NEDF SeaLL1, as a function of the equivalent incident neutron energy in the ^{239}Pu(n, f) reaction along with available experimental data for the reaction ^{239}Pu$(n_{\rm th}, f)$ from Refs. [99–102]. The fragment mass A is before neutron emission.

of $R_T(A)$, which is adjusted to available data (select spontaneous and thermal neutron induced fission reactions). The underlying assumption is consistent with no energy dependence for the CGFM default parametrization, and thus when CGMF calculations are performed, the average multiplicity of neutrons emitted as a function fission fragment mass increases almost uniformly with increasing the incident neutron energy for both light and heavy fragments, as illustrated in Fig. 6(a). However, experimental evidence in U and Np neutron-induced reactions has shown that only for the heavy fragment does the number of neutrons increase [104,105], while the number of neutrons emitted from the light fragments remains constant, within experimental uncertainties. Adding the parametrization of the energy dependence from our TDSLDA calculations, Fig. 6(b) shows that we obtain indeed a very similar trend with what is expected from the experimental data, which suggests that the TDSLDA modeling of the excitation energy sharing between fission fragments is reasonable.

B. Collective flow energy

Certain rather crucial aspects of the nuclear collective motion were never elucidated in a microscopic calculation and were treated only phenomenologically. Is the character of the evolution from saddle to scission adiabatic? If not, is it controlled by the one-body and/or the two-body dissipation, and if so, to what extent? In phenomenological studies, the strength of the one-body dissipation is often artificially reduced and a contribution arising from the two-body dissipation mechanism is included [45].

It is important to remember that the effect of two-body collisions is encoded in the collision integral of the Boltzmann-Uehling-Uhlenbeck equation [106,107]. On the other hand, the evolution equation for the local number density $n(\mathbf{r}, t)$, i.e., the continuity equation $m\dot{n}(\mathbf{r}, t) + \mathrm{div}\,\mathbf{p}(\mathbf{r}, t) = 0$, and the similar equation for the total local linear momentum density $\mathbf{p}(\mathbf{r}, t)$, which includes the momentum flux density tensor, does not involve the collision integral. Thus, the shapes of the mean field and of the nucleon effective mass, determined mostly by $n(\mathbf{r}, t)$, are not directly affected by the two-body collisions. However, the rate of the thermalization of the momentum distribution is controlled by the two-body dissipation mechanism.

The NEDF should satisfy the local Galilean covariance, which implies that the total energy of the system, which is conserved, can be represented as a sum [57,108,109]

$$\begin{aligned} E_{\rm tot} &= E_{\rm coll}(t) + E_{\rm int}(t) \\ &\equiv \int d\mathbf{r} \frac{mn(\mathbf{r}, t)\mathbf{v}^2(\mathbf{r}, t)}{2} \\ &\quad + \int d\mathbf{r}\, \mathcal{E}(\tau(\mathbf{r}, t) - n(\mathbf{r}, t)m^2\mathbf{v}^2(\mathbf{r}, t), n(\mathbf{r}, t), \ldots), \end{aligned} \tag{15}$$

where $n(\mathbf{r}, t)$ is the number density, $\tau(\mathbf{r}, t)$ is the kinetic density, $\mathbf{p}(\mathbf{r}, t) = mn(\mathbf{r}, t)\mathbf{v}(\mathbf{r}, t)$ are linear momentum and local collective and hydrodynamic velocity densities, and ellipses stand for various other densities. $\frac{\mathbf{p}(\mathbf{r},t)}{n(\mathbf{r},t)}$ is the position of the center of the local Fermi sphere in momentum space. The first term in Eq. (15) is the collective and hydrodynamic energy flow $E_{\rm coll}$ and the second term is the intrinsic energy $E_{\rm int}$ in the local rest frame. For the sake of simplicity, we have suppressed the spin and isospin DoF, even though they are included in all the actual calculations. The collective energy $E_{\rm coll}(t)$ is not vanishing only in the presence of currents and vanishes exactly for stationary states. The inertia tensor in $E_{\rm coll}(t)$ in the case of irrotational collective motion is fully equivalent to the Werner-Wheeler inertial tensor [27]. The intrinsic energy $E_{\rm int}(t)$ is determined only by the fermionic matter distribution. A similar partition of the total energy of the nucleus exists in the TDGCM approach; see Sec. II.

We have evaluated the collective flow energy during the saddle-to-scission evolution, see Fig. 7,

$$E_{\rm coll}(t) = \int d\mathbf{r} \frac{mn(\mathbf{r}, t)\mathbf{v}^2(\mathbf{r}, t)}{2} = \int d\mathbf{r} \frac{|\mathbf{p}(\mathbf{r}, t)|^2}{2mn(\mathbf{r}, t)}, \tag{16}$$

which is a quantity unaffected by two-body collisions. In the case of pure adiabatic evolution—as in TDGCM or ATDHF,

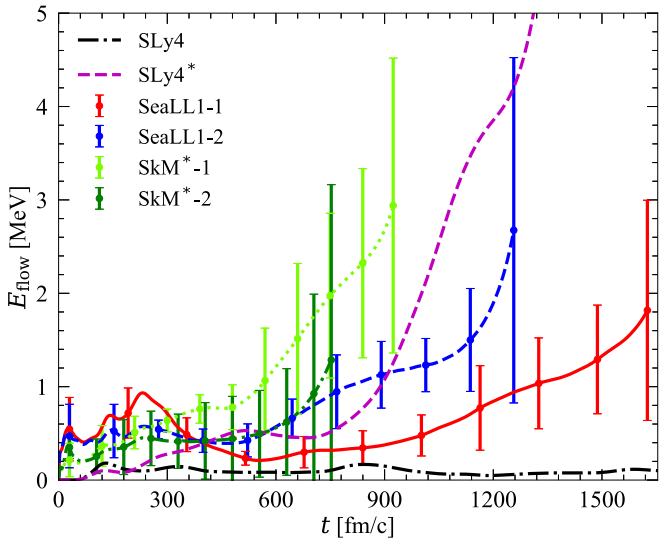

FIG. 7. The collective flow energy evaluated for NEDFs with realistic pairing SLy4 [62] (dash-dotted line), enhanced pairing SLy4* (dashed line), SkM*(dotted and dash-doted lines with error bars), and SeaLL1 (solid and dashed lines with errors bars) sets. The error bars illustrate the size of the variations due to different initial conditions in the cases of SeaLL1-1,2 and SkM*-1,2 NEDFs. In the case of enhanced pairing NEDF Sly4*, the time has been scaled by a factor of 1/10.

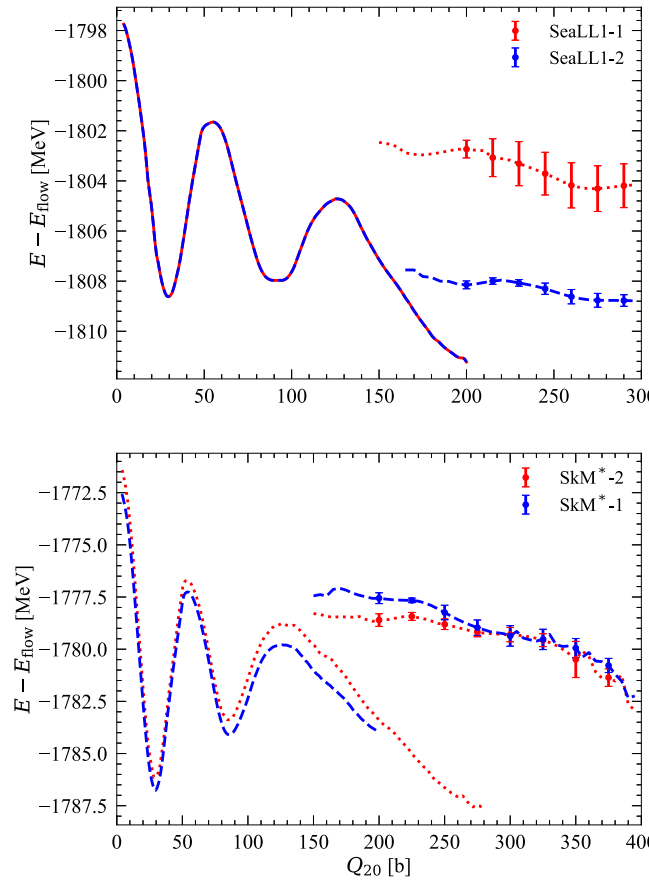

FIG. 8. The intrinsic energy $E_{\rm int}(t)$ along the fission path for SeaLL1-1 (dotted line with error bars) and SeaLL1-2 in the upper panel and SkM*-2 (dash line with error bars) and SkM*-1 (dotted line with error bars) in the lower panel. The error bars illustrate the size of the variations due to different initial conditions in the cases of SeaLL1-1,2 and SkM*-1,2 NEDFs. The collective potential energy determined in a constrained calculation, see Eq. (5), is represented in both panels with either dotted or dashed lines for the corresponding SeaLL1 and SkM* NEDFs. In the case of an adiabatic evolution along the fission path, $E_{\rm int}(t)$ would trace rather closely the collective potential energy determined in the constrained calculation. Scission configuration corresponds to a quadrupole momentum of the entire nuclear system $Q_{20} \approx 400$ b.

see Sec. II—one expects a full conversion of the collective potential energy into a collective flow energy of ≈15–20 MeV.

Surprisingly, our simulations point to an unexpectedly small $E_{\rm coll}$ from saddle to scission, corresponding to a collective speed $\frac{v_{\rm coll}}{c} \approx 0.002$–$0.004$, significantly smaller than the Fermi velocity $\frac{v_F}{c} \approx 0.25$; see Figs. 7 and 8. Since in TDDFT one simulates the one-body dynamics exactly, it is natural to discuss adiabaticity at the mean-field level. The transition rate between sp states is suppressed if the time to cross an avoided level-crossing configuration satisfies the restriction $\Delta t \ll \frac{\hbar}{\Delta\epsilon} \approx 400\,{\rm fm/c}$, where $\Delta\epsilon = \frac{1}{\rho_{\rm sp}(\epsilon_F)}$ is the average sp energy level spacing at the Fermi level. Since on the way from saddle-to-scission several dozen of avoided level crossings occur [78,80], this condition is clearly violated. The collective motion is thus expected to be strongly overdamped. From saddle to scission, the nucleus behaves as a very viscous fluid, the role of collective inertia is strongly suppressed, and the trajectories follow predominantly the direction of the steepest descent with the terminal velocity determined by the balance between the friction and the driving conservative forces; see Fig. 5.

This result serves as the first microscopic justification for the assumption of the overdamped Brownian motion model [43] and partially to the scission-point model [50–52]. In both these phenomenological models, it is assumed that the preformed FF are in thermal equilibrium and that the collective energy flow is either vanishing or very small. The main difference is that in the scission-point model there is no mechanism to ensure that all equilibrium scission configurations could be reached dynamically, while the nucleus evolves from the saddle to scission. It is equally surprising that in the case of enhanced pairing, when the pairing condensates retain their long-range order throughout the entire saddle-to-scission evolution, the collective dynamics has the same general characteristics.

The present results put a lower limit on the role of the viscosity on fission times, as fluctuations can only lead to longer trajectories [25]. The character of the collective dynamics unveiled here suggests that in physically realistic Langevin [43,45–48] and TDGCM [29,30] studies the dynamics of the intrinsic DoF should be generated at (an approximately) fixed intrinsic energy, since $E_{\rm coll}(t)$ is small up to scission. If the thermalization of the intrinsic DoF is achieved quickly enough and if the temperature of the system were constant, the force driving the collective dynamics is

determined by the free energy gradient [24]

$$\boldsymbol{F}_{\boldsymbol{Q}} = -\boldsymbol{\nabla}_{\boldsymbol{Q}}[E_{\rm int}(\boldsymbol{Q},T) - TS(\boldsymbol{Q},T)] \approx \boldsymbol{\nabla}_{\boldsymbol{Q}}[TS(\boldsymbol{Q},T)], \tag{17}$$

where $S(\boldsymbol{Q},T)$ is the entropy and

$$E_{\rm tot} = E_{\rm int}(\boldsymbol{Q},T) + E_{\rm coll}(t) \approx E_{\rm int}(t). \tag{18}$$

However, as our results show, the "temperature" of the nucleus, while descending from the saddle to scission increases, as $E_{\rm int}(t) \approx$ const. In that case, for each set of the collective variables $\boldsymbol{Q}$, the temperature T shall be adjusted so that $E_{\rm int}(\boldsymbol{Q},T)$ remains practically equal to its starting value, due to the smallness of $E_{\rm coll}(t)$. The intrinsic DoF carry most of the intrinsic entropy of the fissioning nucleus and that drives the fission dynamics until scission. The entropy $S(\mathbf{Q},T)$ and the temperature are peaked along the bottom of the fission valley and there the free energy $\mathcal{F}(\mathbf{Q},T) = E_{\rm int}(\boldsymbol{Q},T) - TS(\boldsymbol{Q},T)$ reaches a minimum for fixed $\mathbf{Q}$, where one expects to find the most probable fission path between the outer saddle and the scission configuration.

In order to include fluctuations, one can proceed in at least two different ways. One possible avenue is to follow the procedure described in Ref. [25]. An alternative approach is to introduce an appropriate number of collective variables $\boldsymbol{Q}$, minimize the grand canonical ensemble with respect to the sp DoF

$$\Omega = \min[E_{\rm int}(\boldsymbol{Q},T) - TS(\boldsymbol{Q},T) - \mu_N N - \mu_Z Z - \boldsymbol{\lambda}\cdot\boldsymbol{Q}], \tag{19}$$

and additionally vary the temperature until the constraint

$$E_{\rm tot} \approx E_{\rm int}(\boldsymbol{Q},T) \tag{20}$$

is satisfied, where $E_{\rm tot}$ is the initial total energy of the fissioning nucleus. At this point, one would choose to make a step in the collective variable space

$$\boldsymbol{Q} \to \boldsymbol{Q}_{\rm new} = \boldsymbol{Q} + \delta\boldsymbol{Q} \tag{21}$$

and determine the new temperature $T_{\rm new}$ as well by accepting or rejecting the new values $\boldsymbol{Q}_{\rm new}$ according to the Metropolis criterion for the ratio between the level densities of the old $\rho(\boldsymbol{Q})$ and new $\rho(\boldsymbol{Q}_{\rm new})$ configurations, with probability

$$P(Q \to Q_{\rm new}) = \min\left[\frac{\rho(\boldsymbol{Q}_{\rm new})}{\rho(\boldsymbol{Q})}, 1\right] \approx \min\{\exp[S(\boldsymbol{Q}_{\rm new},T_{\rm new}) - S(\boldsymbol{Q},T)], 1\}. \tag{22}$$

C. Relaxation of the collective degrees of freedom

To demonstrate the overdamped character of the fission dynamics, we performed the following theoretical experiment. We have applied at random times, the red dots in Fig. 9, collective kicks to the nucleus of random intensities η according to the prescription

$$\begin{pmatrix} u_{k\sigma}(\boldsymbol{r},t) \\ v_{k\sigma}(\boldsymbol{r},t) \end{pmatrix} \to \begin{pmatrix} \exp[+i\eta\phi(\mathbf{r})]u_{k\sigma}(\boldsymbol{r},t) \\ \exp[-i\eta\phi(\mathbf{r})]v_{k\sigma}(\boldsymbol{r},t) \end{pmatrix}, \tag{23}$$

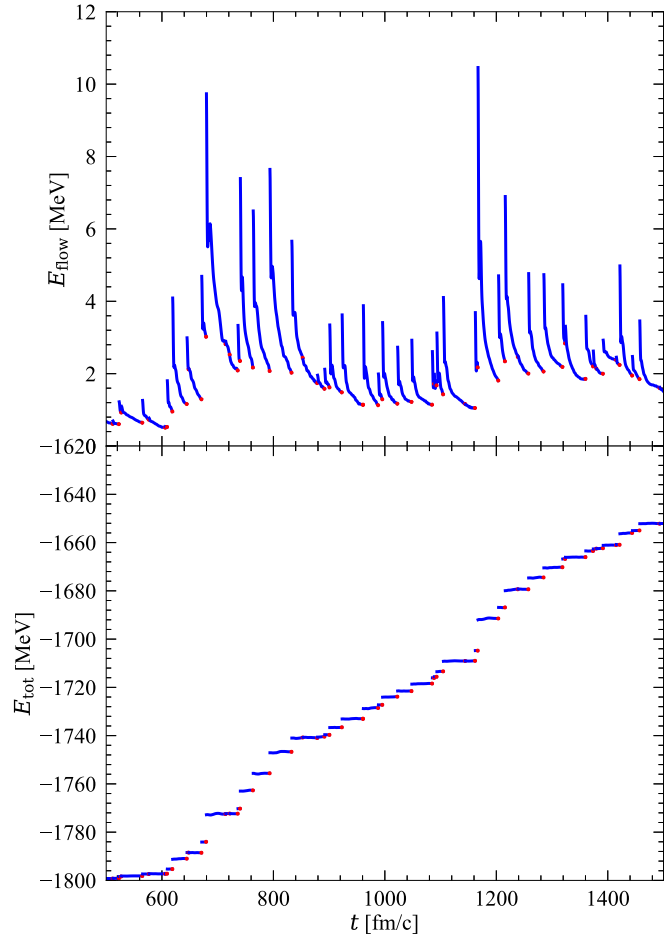

FIG. 9. Upper panel: At times indicated with red dots we have applied collective quadrupole momentum kicks to both neutrons and protons, see Eq. (23), with random values of η. Lower panel: The time evolution of the total energy of the nucleus, in the rest frame of the nucleus, after we have applied collective kicks to both neutrons and protons with random values of η.

where $\sigma = \uparrow, \downarrow$, which immediately resulted in an increase of the collective flow energy only. The momenta of all nucleons are instantaneously shifted by the same amount $\Delta\mathbf{p} = \hbar\eta\boldsymbol{\nabla}\phi(\mathbf{r})$ and the excitation energy injected into the nucleus by a such a collective kick is

$$\Delta E = \int d\mathbf{r} n(\mathbf{r}) \left[\frac{|\eta\hbar\boldsymbol{\nabla}\phi(\mathbf{r}) + m\mathbf{v}(\mathbf{r},t)|^2}{2m} - \frac{m|\mathbf{v}(\mathbf{r},t)|^2}{2}\right], \tag{24}$$

where $n(\mathbf{r})$ is the total number density and $\mathbf{v}(\mathbf{r},t)$ is the local collective velocity prior to the kick. Immediately after such a kick, the density distribution has the same profile as just before the kick, as the phase of the qpwfs do not affect number densities but affect the currents and the kinetic energy density. After a relatively short time, of the order of a few tens fm/c, this excess collective flow energy is rapidly dissipated into intrinsic DoF and the nucleus is thus heated up. This added energy is never returned into the collective flow energy of the fissioning nucleus. After each collective "kick," the intrinsic energy of the nucleus increases; see Fig. 9. Even though the

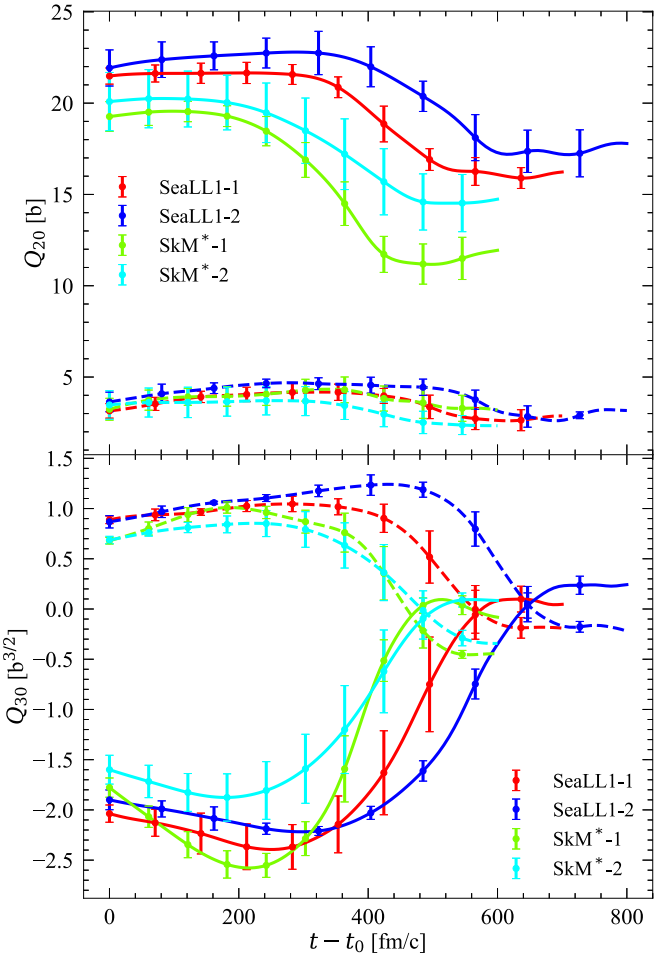

FIG. 10. The evolution of the quadrupole Q_{20} and octupole Q_{30} moments of the light (solid lines) and heavy (dashed lines) FFs before and after scission. The time t_0 stands for the moment when the distance between the two fragments is about 15 fm and the neck of mother nucleus is formed. Scission occurs at $t - t_0 \approx 300$ fm/c. The solid lines represent the multipoles moments of the light fragment and the dashed lines show the multipole moments of the heavy fragment in the case of the SeaLL1-1,2 and SkM*-1-2 respectively. The error bars illustrate the size of the variations due to different initial conditions in case of SeaLL1-1,2 and SkM*-1,2 NEDFs.

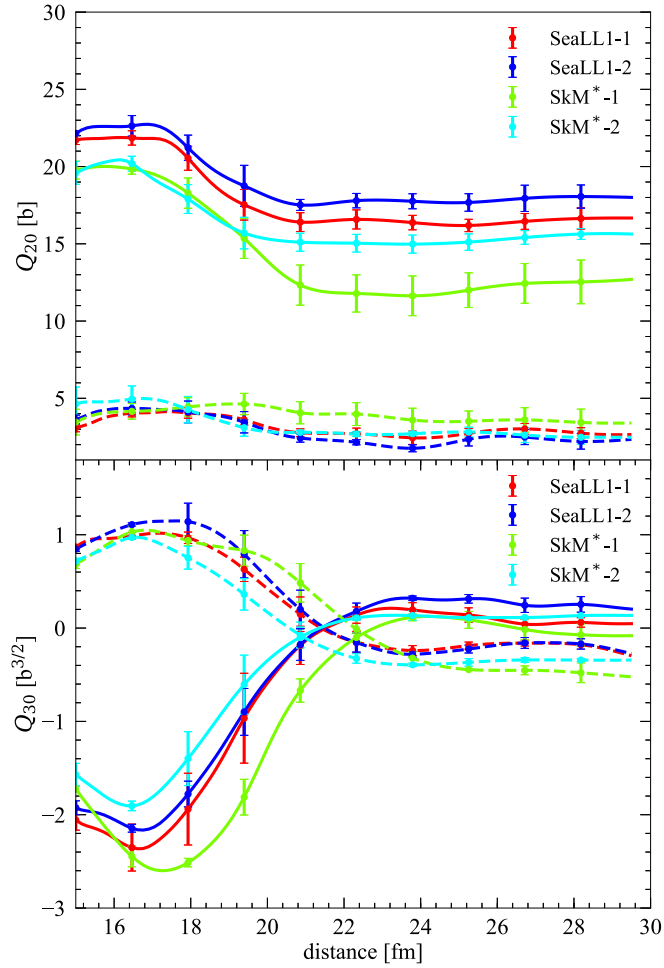

FIG. 11. The evolution of the quadrupole Q_{20} and octupole Q_{30} moments of the light (solid lines) and heavy (dashed lines) FFs before and after scission, here as a function of the separation between the FFs. At scission, the separation between the FFs is ≈17 fm. The meaning of various lines and error bars are explained in the caption to Fig. 10.

intrinsic energy increased by ≈150 MeV after many collective kicks, the rate at which the additional energy in absorbed does not visibly change. This serves as an additional argument that the one-body dissipation mechanism is very effective in bringing the collective flow velocity to the terminal velocity, which is achieved when the friction force cancels the driving force; see also the discussion in Appendix C.

D. Shape relaxation of fission fragments

The one-body dissipation is important both before and after scission. The light fragment at scission is very elongated and both fragments have also a noticeable amount of octupole deformation, very different than the corresponding moments in the ground state. In Fig. 10, we show the evolution of Q_{20} and Q_{30} for both FFs after scission. All these moments relaxed rather rapidly, without performing any oscillations to the values very close to the ground-state values. Remember, however, that both FFs are not cold. The absence of shape oscillations is another strong indication that one-body dissipation is strong and that even the individual FFs LACM is overdamped always. The relatively large quadrupole deformation energy of the light fragment is thus converted into heat and its quadrupole moment is considerably reduced. Both fragments are octupole deformed at scission, and these octupole moments relax to relatively small values. As the deformation energy is converted into intrinsic excitation energy, the temperatures of both FFs increase, compared to the corresponding temperatures at scission. In Fig. 11, we plot the evolution of these quadrupole and octupole moments as a function of the separation between the FFs. The FFs achieve their relaxed shapes at a separation between FFs ≈22 fm, when the distance between their tips is about 4 to 5 fm. This FFs separation at which their shapes are relaxed is noticeably larger than the separation considered in

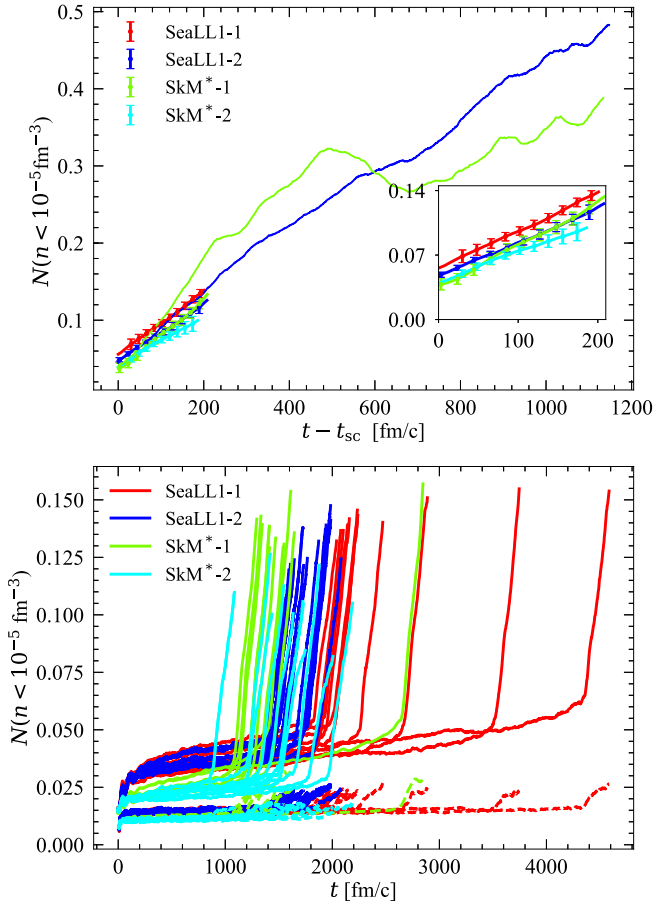

FIG. 12. Upper panel: The number of neutrons emitted predominantly after scission. The error bars quantify the size of the fluctuations between trajectories corresponding to different initial conditions. Lower panel: the number of neutrons as a function of time emitted in each trajectories in the inset of upper one.

the scission-point model [50–52] or in the Brownian motion model [43,44,53–55].

E. Neutrons emitted by fission fragments

Neutron emission is an important mechanism in the deexcitation of FF. We have also estimated the neutron emission rates before the FFs are fully separated, 4.0×10^{-4} neutrons/(fm/c), which are rather stable with respect to the variation of initial conditions, deformation, initial energy, or NEDF. By the time the FFs reach a separation of ≈60 fm, we find that about 0.4 neutrons are emitted on average, in fair agreement with theoretical estimates [110,111] and with experimental hints of neutrons emitted before full acceleration [112–115].

In Fig. 12, we show the number of neutrons in the volume where the number density $n(\boldsymbol{r}, t) \leqslant 10^{-5}$ fm^{-3} as a function of time after scission for all the fission trajectories we have evaluated. The neutron emission rates (the slopes) demonstrate a robust independence on the initial conditions or the NEDF used. These neutrons are emitted preferentially parallel to the FFs motion, a conclusion likely affected by the finite transverse size of simulation boxes.

VI. CONCLUSIONS

The present study is the first in the literature in which no restrictions have been imposed on the mean-field dynamics and the pairing field was treated beyond the BCS approximation. In TDHF+BCS treatments reported so far in the literature, a relatively low-energy cutoff was always imposed on the energy band where pairing correlations are active. Arguments are often presented that such a limited space for pairing correlation is sufficient, as the energy gain is reproduced with enough accuracy. However, as Anderson notes [116] (see page 128) when he discusses the "quantum chemists' fallacy no. 1 and 2," of which even Wigner was partially guilty, "you may get pretty good energetics out of a qualitatively wrong state." The perfect example is the case of a superconductor, in which in spite of the fact that the contribution from the condensation energy is negligible, the wave function with pairing correlations leads to qualitative changes.

It is well known that pairing correlations in nuclei, unlike in superconductors, are mostly due to short-range attractive forces, and that is inconsistent with the assumption that pairing correlations are active in a narrow energy window only. In particular, this is also true for the popular finite-range Gogny interaction [117], in which case the pairing cutoff energy could be as high as $O(100)$ MeV. The contribution of the pairing correlations to the total energy of the nucleus is very modest and varying the energy window where these correlations are active is not going to influence noticeably the total energy. However, the total nuclear wave function is affected significantly by the size of the energy window in which the pairing correlations are allowed to participate, particularly in dynamics. As we do not implement any arbitrary energy cutoff on pairing correlations, we are able to perform an accurate microscopic test on whether the LACM fission dynamics is indeed adiabatic in character.

Adiabaticity in LACM is typically conflated with slowness of the collective motion [27,28,34–37], an assumption which allows one to introduce collective DoF which are decoupled from the intrinsics DoF and also legitimizes the introduction of a collective Hamiltonian. Until now, the validity of this assumption has not been checked, since the required simulations exceeded the computer capabilities of previous researchers. The only previous serious attempt we are aware of is due to Ledergerbert *et al.* [118], who, however, were unable to arrive at a conclusive decision, basically because the phase space they were able to consider at the time was incontrovertibly too small.

The one-body dissipation mechanism has been suggested by Blocki *et al.* [26] and almost three decades earlier by Fermi [119], under a different name, in order to explain the energy spectrum of cosmic rays. Fermi suggested that charged particles (protons) collide with moving magnetic fields and as a result are accelerated to very large energies. The energy from the moving magnetic fields, which play a similar role to the moving nuclear surface, is transferred to the charged particles (protons), which play a similar role to the intrinsic nucleonic DoF. In a nucleus, which is a finite system, the intrinsic DoF bring the nuclear walls almost to a standstill, as present results manifestly demonstrate.

One-body dissipation is automatically incorporated in TDDFT and it was conjectured for many years to be important in LACM. Negele *et al.* [120] concluded that one-body dissipation is important in fission dynamics, based, however, on studying only three TDHF trajectories for fission of ^{238}U, with three values for a *static* (sic) pairing field with the pairing gaps $\Delta = 0.7$, 2.0, and 6.0 MeV and comparing these results with classical Langevin simulation of fission dynamics, with one-body dissipation estimated for a Fermi gas model. Notably, the kinetic energy of the FFs at scission determined in this TDHF study was about 11–12 MeV, an order of magnitude larger than the value we determine and also a value consistent with adiabatic character of the large-amplitude collective motion from saddle to scission, which we dispute here. From this type of comparison, these authors concluded that one-body dissipation is important in fission dynamics. Over the years, the practitioners of the Langevin type of simulations have claimed that both one-body and two-body dissipation are important in low-energy fission dynamics [24,45–48], using phenomenologically adjusted dissipation coefficients, though it is not always clear how one can disentangle the two forms of dissipation; see, e.g., the study performed by Sierk [45]. Not all Langevin implementations are compatible with one another, though the level of agreement with data is about the same. Moreover, there are TDGCM simulations [30,121], in which the nature of fluctuations is qualitatively different, quantum in character, but the quality of the agreement with experiment for FFs mass yields are comparable with those achieved in Langevin approaches, where the fluctuations are thermal in character. All this might suggest that the FFs mass yields are likely not very sensitive to the nature and details of various fluctuations models.

In the last few years Randrup and collaborators [43,44,53–55] took this assumption to the extreme and suggested that fission dynamics is actually overdamped and one should replace the Langevin approach with the Smoluchowski approach. In this case, the role of the collective inertia becomes irrelevant and a more accurate description of the fission yields, the TKE, and the sharing of the TXE can be achieved. This approach shares similarities with the scission point model [50–52], as both approaches assume total conversion of the saddle-to-scission collective potential energy difference into the FF's intrinsic excitation energy or, in other words, into heat. As we demonstrate here, however, these phenomenological models neglect the fact FFs fragments attain their equilibrium shapes when they are quite well separated and thus they underestimate the excitation energy of the FFs. From the scission configuration to the point where the FFs reach their equilibrium shapes, the deformation energy of the FFs is converted into additional internal excitation energy.

We have shown in Sec. V C that at scission both FFs emerge with significant quadrupole and octupole deformations, which relax to their equilibrium values only after the FFs are significantly separated; see Figs. 10 and 11 below. The "surplus" deformation energies of the FFs are converted into additional internal excitation energies of the FFs, on top of their "thermal" excitation energy achieved during the descent from saddle to scission, and it affects the average neutron multiplicity spectra, which are emitted by the fully accelerated FFs; see Fig. 6. No phenomenological models so far incorporated these aspects, particularly the octupole deformations of the emerging FFs at scission. As a result, these phenomenological models underestimate the magnitude of the excitation energies of the FFs and consider only an oversimplified excitation energy mechanism between FFs.

If dissipation is important and moreover overdamped in fission dynamics, the introduction of collective DoF freedom, of a potential energy surface and of a collective inertia, and the decoupling of the DoF into collective and intrinsic parts become highly questionable. We have established that one-body dissipation is very strong and that in fission LACM is strongly overdamped under almost any reasonable assumptions. Under such circumstances, the role of "collective inertia" becomes irrelevant and the theoretical arguments in favor of a TDGCM/ATDHF approach or Langevin approach become questionable as well, along with the mere definition of collective variables, as a collective Hamiltonian by definition describes a nondissipative motion.

We have determined that the memory of the initial conditions near the outer barrier are rather quickly forgotten, in a relaxation time $\tau_{\rm relax} \approx O(50)$ fm/c. As the saddle to scission is $\tau_{s\to s} \approx O(10^3$–$10^4)$ fm/c, the widths of the FFs mass, charge, TKE, TXE, and spin distributions are determined during this relatively fast nonequilibrium evolution interval from saddle to scission, due to the presence of non-negligible fluctuations. During this interval of time, practically the entire gain in potential energy of a nucleus sliding down from the saddle to scission is converted into internal heat.

We have used three different NEDFs (SLy4, SeaLL1, and SkM*), along with variations in treatment of the pairing correlations, and our conclusions are quite robust. All these NEDFs satisfy basic constraints: The nuclear matter is liquid in nature (thus mostly incompressible) and characterized by a significant surface tension and isospin asymmetry due to a strong Coulomb interaction, and the spin-orbit and the pairing correlations have realistic values. When all these basic requirements are satisfied, the emerging most likely values for the TKE, atomic, and charge numbers are in agreement with experiment without the need of any additional fitting. In addition, we were able to extract the excitation energy sharing between the FFs. Depending on the initial energy of the fissioning nucleus, the excitation energy-sharing changes in a manner which appears to be in agreement with experimental data on average neutron multiplicities.

Many other quantities of interest for various applications could also be extracted, such as the angular momentum distributions of the FFs and their parities [122,123].

The only disadvantage of the present approach is that it lacks fluctuations, which likely could be later added [25]. Upon introductions of fluctuations, one should be able extract FFs mass, charge, TKE, and TXE distributions.

ACKNOWLEDGMENTS

We are grateful to G. F. Bertsch for numerous discussions and helpful comments on the manuscript and to P. Magierski for a number of suggestions to improve the narrative. We

thank I. Abdurrahman for helping to prepare Fig. 1. The work of A.B. and S.J. was supported by US Department of Energy, Office of Science, Grant No. DE-FG02-97ER41014 and in part by NNSA Cooperative Agreement No. DE-NA0003841. The TDDFT calculations have been performed by S.J. at the OLCF Summit, Titan, and Piz Daint and S.J. generated initial configurations for direct input into the TDDFT code at OLCF Titan and Summit and NERSC Edison. This research used resources of the Oak Ridge Leadership Computing Facility, which is a US DOE Office of Science User Facility supported under Contract No. DE- AC05-00OR22725, and of the National Energy Research Scientific computing center, which is supported by the Office of Science of the US Department of Energy under Contract No. DE-AC02-05CH11231. We acknowledge PRACE for awarding us access to resource Piz Daint based at the Swiss National Supercomputing Centre (CSCS), Decision No. 2016153479. The work of K.J.R. is supported by US DOE Office of Advanced Scientific Computing Research and was conducted at Pacific Northwest National Laboratory and University of Washington. The work of N.S. was supported by the Scientific Discovery through Advanced Computing (SciDAC) program funded by the US Department of Energy, Office of Science, Advanced Scientific Computing Research and Nuclear Physics, and it was partly performed under the auspices of the US Department of Energy by the Lawrence Livermore National Laboratory under Contract No. DE-AC52-07NA27344. N.S. performed the calculations of the initial configurations and of the temperatures of the FFs. Some of the calculations reported here have been performed with computing support from the Lawrence Livermore National Laboratory (LLNL) Institutional Computing Grand Challenge program. The work of I.S. was supported by the US Department of Energy through the Los Alamos National Laboratory. Los Alamos National Laboratory is operated by Triad National Security, LLC, for the National Nuclear Security Administration of U.S. Department of Energy (Contract No. 89233218CNA000001).

APPENDIX A: NUMERICAL IMPLEMENTATION

In the present study, we have significantly increased the size of the simulation box compared to our proof-of-principle results of Ref. [62], from $22.5^2 \times 40$ to $30^2 \times 60$ fm^3, using the same lattice constant $l = 1.25$ fm, which corresponds to a momentum cutoff $p_c = \frac{\hbar\pi}{l} \approx 500\,\mathrm{MeV/c}$ in each spatial direction. The momentum space is in this case a cube with volume $(2p_c)^3$. The total number of available quantum sp states is thus

$$\mathcal{N}_{qs} = 4\frac{N_x N_y N_z l^3 (2p_c)^2}{(2\pi\hbar)^3} = 4N_x N_y N_z = 110\,592, \tag{A1}$$

where the factor 4 accounts for the spin and isospin DoF. This significant increase in the size of the calculations was required in order to ensure numerical stability in larger spatial lattices [124]. We use fast Fourier transform (FFT) to compute spatial derivatives, since it reduces the number of floating point operations significantly while practically ensuring machine precision for derivatives. We avoid computing first-order derivatives when possible; e.g., we take advantages of standard relationships such as

$$\begin{aligned}&\nabla F(\boldsymbol{r})\cdot\nabla G(\boldsymbol{r})\\ &\quad\to \tfrac{1}{2}\{\Delta[F(\boldsymbol{r})G(\boldsymbol{r})] - \Delta[F(\boldsymbol{r})]G(\boldsymbol{r}) - F(\boldsymbol{r})\Delta[G(\boldsymbol{r})]\}\end{aligned} \tag{A2}$$

for increased numerical accuracy. The evaluation of first-order derivatives requires the elimination of the highest frequency in the Fourier transform for numerical accuracy. If couplings to gauge fields is required, as in Ref. [125], or when evaluating terms linear in momentum, we use the discretized symmetrized form

$$\begin{aligned}&\boldsymbol{A}(r,t)\cdot\nabla\psi(\boldsymbol{r},t)\\ &\quad\to \tfrac{1}{2}[\boldsymbol{A}(r,t)\cdot\nabla\psi(\boldsymbol{r},t) + \nabla\psi(\boldsymbol{r},t)\cdot\boldsymbol{A}(r,t)].\end{aligned} \tag{A3}$$

When evaluating first-order derivatives of products of functions, we use Leibniz rule

$$\nabla[A(\boldsymbol{r})B(\boldsymbol{r})] \to\ B(\boldsymbol{r})\nabla A(\boldsymbol{r}) + A(\boldsymbol{r})\nabla B(\boldsymbol{r}). \tag{A4}$$

The use of this rule is particularly important to ensure numerically accurate gauge invariance. As discussed in Refs. [60,126], with a careful choice of the size of the box and of the spatial lattice constant one can achieve very high numerical accuracy with relatively large values of lattice constant l. In computing the Coulomb potential, we use the method described in Ref. [127] to solve the Poisson equation in order to eliminate the contributions from images, which are inherent when using periodic boundary conditions.

The initial state is generated using the code HFBTHO [61] with appropriate constraints on the expectation value of the quadrupole $\langle\hat{Q}_{20}\rangle$ and octupole $\langle\hat{Q}_{30}\rangle$ moments. HFBTHO calculations are performed in a stretched basis of $N_0 = 28$ shells with the deformation β and the oscillator frequency ω_0 set as in Ref. [72]. The matrix of the Bogoliubov transformation is then transformed in the coordinate space representation on a spatial lattice of size $N_x N_y N_z \times N_x N_y N_z$ according to

$$\begin{pmatrix} u_{k\sigma}(\boldsymbol{r}) \\ v_{k\sigma}(\boldsymbol{r}) \end{pmatrix} = \begin{pmatrix} \sum_n U_{nk}\psi_{n\sigma}(\boldsymbol{r}) \\ \sum_n V_{nk}\psi^*_{n\sigma}(\boldsymbol{r}) \end{pmatrix}, \tag{A5}$$

where $\psi_{n\sigma}(\boldsymbol{r})$ are the harmonic oscillator basis spinors; see Refs. [128,129]. The qpwfs are used to reconstruct the densities and the potentials, with the help of which we construct the initial conditions in Eq. (8) (in total $4N_x N_y N_z$ neutron and proton qpwfs) by diagonalizing the full pairing Hamiltonian matrix, including the constraints

$$\begin{aligned}&\begin{pmatrix} h_{\uparrow\uparrow}-q & h_{\uparrow\downarrow} & 0 & \Delta \\ h_{\downarrow\uparrow} & h_{\downarrow\downarrow}-q & -\Delta & 0 \\ 0 & -\Delta^* & -h^*_{\uparrow\uparrow}+q & -h^*_{\uparrow\downarrow} \\ \Delta^* & 0 & -h^*_{\downarrow\uparrow} & -h^*_{\downarrow\downarrow}+q \end{pmatrix}\begin{pmatrix} u_{k\uparrow} \\ u_{k\downarrow} \\ v_{k\uparrow} \\ v_{k\downarrow} \end{pmatrix}\\ &\quad = E_k\begin{pmatrix} u_{k\uparrow} \\ u_{k\downarrow} \\ v_{k\uparrow} \\ v_{k\downarrow} \end{pmatrix},\end{aligned} \tag{A6}$$

where $q = \sum_l \lambda_l Q_{l0}$ stands for all constraints, including the corresponding Lagrange multipliers.

A larger simulation box allows us to more precisely characterize the FFs properties. The sp level density is denser, and during the dynamics sp states mix more easily. This forced us to include all sp levels in the simulations, in order to avoid numerical instabilities for long-time trajectories, due to level crossings. This also led to a slightly modified renormalization procedure of the pairing gap constant, using Eqs. (5.47)–(5.50) from Ref. [130], in a similar manner to what was described in Refs. [56,131,132]

$$\frac{1}{g_{\rm eff}} = \frac{1}{g} - \frac{2.442\, m}{4\pi\hbar^2 l}, \tag{A7}$$

where l is the lattice constant. The number of coupled nonlinear time-dependent three-dimensional (3D) partial differential equations (PDEs) solved increased significantly from ≈56 000 in Ref. [62] to $16 \times N_x N_y N_z = 442\,368$ PDEs for a typical lattice $N_x N_y N_z = 24^2 \times 48$. While evaluating the neutron emission rates, we have used in a couple of instances an even larger simulation box $30^2 \times 120$ fm^3, which amounted to evolving in time 884 736 PDEs.

The larger cutoff energy and the larger number of PDEs required a smaller time-step integration $\Delta t = 0.03$ fm/c, leading to an error $\epsilon \sim (E_{\rm cut}\Delta t/\hbar)^6$, which is required per time step for the predictor, modifier, and corrector steps, and where the maximum $E_{\rm cut} = (3p_c^2/2m)$. We use the Adams-Bashforth-Milne predictor-modifier-corrector time-integration algorithm [133]:

$$p_{n+1} = \frac{y_n + y_{n-1}}{2} + \frac{h}{48}(119\mathbf{y}'_n - 99y'_{n-1} + 69y'_{n-2} - 17y'_{n-3}) + \frac{161}{480}h^5 y^{(5)}, \tag{A8}$$

$$m_{n+1} = p_{n+1} - \frac{161}{170}(p_n - c_n) + \frac{923}{2880}h^6 y^{(6)}, \tag{A9}$$

$$c_{n+1} = \frac{y_n + y_{n-1}}{2} + \frac{h}{48}(17\mathbf{m}'_{n+1} + 51y'_n + 3y'_{n-1} + y'_{n-2}) - \frac{9}{480}h^5 y^{(5)}, \tag{A10}$$

$$y_{n+1} = c_{n+1} + \frac{9}{170}(p_{n+1} - c_{n+1}) - \frac{43}{2880}h^6 y^{(6)}, \tag{A11}$$

where we have indicated with a bold symbol the only two times during a time step when the right-hand side of the differential equation has to be evaluated, namely $\mathbf{y}'_n$ for p_{n+1} and $\mathbf{m}'_{n+1}$ for c_{n+1}. The scheme has an overall accuracy of $\epsilon \sim (E_{\rm cut}\Delta t/\hbar)^6 = 5 \times 10^{-10}$ per time step. It also requires only two evaluations of the right-hand side of Eq. (8), namely only two applications of the Hamiltonian on the qpwfs. To start the propagation and to checkpoint restart a previous calculation, we use a Taylor expansion of the unitary mean field propagator. With such a time step, the particle number is conserved practically with machine precision and the total energy with an error ≈0.25–0.5 MeV for trajectories as long as 3 000 fm/c and thus 100 000 time steps; see Table III. Our codes use double precision. In starting calculations or after checkpoint or restart, we use for the first four time steps an expansion of the time-ordered sp propagator, similar to the method used in Ref. [134].

TABLE III. The absolute and relative errors of total energy for each set of runs and their corresponding variances in parentheses.

NEDF	$\lvert\delta E\rvert$ [MeV]	$\lvert\delta E/E\rvert$ (%)
SeaLL1-1	0.61(0.29)	0.03(0.01)
SeaLL1-2	0.46(0.12)	0.03(0.01)
SkM*-1	1.03(0.16)	0.06(0.01)
SkM*-2	0.27(0.14)	0.02(0.01)

As mentioned above, the size of the discretized Hamiltonian in Eq. (8) is $4N_xN_yN_z \times 4N_xN_yN_z$, where N_x, N_y, N_z are the number of lattice points in the corresponding spatial directions. Each qpwf has four components and thus one has to solve $16N_xN_yN_z$ partial differential equations (PDEs), where each function is defined on $N_xN_yN_z$ lattice points. Over the years, we have developed a highly efficient code which takes full advantage of the graphics processing unit (GPU) accelerators (using compute unified device architecture (CUDA) programing) and which provides a significant speed-up with respect to a CPU-only code.

The simulations were performed on Titan at OLCF, Oak Ridge, USA, and Piz Daint in Lugano, Switzerland, using a GPU code written in CUDA. A node on Titan has 1 GPU and 16 CPUs. A GPU code on Titan is about 9.4 times faster than a CPU code written in C using the same number of nodes. This speed-up is practically equal to the theoretical limit of Titan. On Piz Daint, the same GPU code is about 3 times faster than on Titan. A fission trajectory of ≈3 000 fm/c, using 512 GPUs on Piz Daint, requires less than 10 wall-time hours, with an excellent strong scaling. The code was also benchmarked on Summit at OLCF, Oak Ridge, USA, and TSUBAME, at Tokyo Institute of Technology, Japan.

We have compared the efficiency of our code with that of the-state-of-the-art codes in literature for TDHF calculations [134,135]; see Table IV. The TDHF Sky3D code [134] evolves at most ≈1 000 PDEs for the collision of two heavy ions, treating pairing correlations within the BCS approximation. The wall time using a number of CPUs equal to the number of GPUs in our approach is almost 100 times longer for similarly sized problems. It is not entirely clear how to compare codes written to solve somewhat different problems, TDHF and TDHFB, for example. As a measure, we have used the required computation time per lattice point of one of the components of a single qpwf, when performing a complete calculation of all the qpwfs,

$$\text{Cost} = \frac{(\#\ \text{CU}) \times (\text{wall time})}{(\#\ \text{time steps}) \times (\#\ \text{PDEs}) \times (\#\ \text{lattice points})}, \tag{A12}$$

where # CU stands for the number of computing units, either CPUs in case of the TDHF codes or GPUs in case of the TDSLDA code. We attribute the superior performance of the TDSLDA solver to the use of a more efficient while very accurate time-integration algorithm, as well as to the use of GPUs. The use of highly efficient and precise FFT for the computation of spatial derivatives could also be a factor. Since in our calculations we have to manipulate large

TABLE IV. Comparison of different existing codes for performing TDDFT calculations on a variety of architectures. The TDSLDA code demonstrates an almost perfect strong scaling on Piz Daint (Lugano) and Summit (Oak Ridge), where further significant optimizations are likely. TDSLDA-opt is an optimized version of our GPU code which reduces the number of calls to CPU-based routines. TDSLDA-simp is a simplified and unoptimized version of our GPU code, performing the same type of calculations as codes [134,135] used in literature for TDHF+TDBCS simulations.

Code	CUs	Computer	PDEs	Lattice	Cost (s)
Sky3D [134]	128	Titan	1 024	$18^2 \times 30$	3.86×10^{-6}
U&S [135]	16	Linux cluster	714	$40^2 \times 70$	8.72×10^{-5}
TDSLDA	514	Titan	442 368	$24^2 \times 48$	4.35×10^{-8}
TDSLDA	240	Piz Daint	442 368	$24^2 \times 48$	1.61×10^{-8}
TDSLDA-opt	240	Piz Daint	442 368	$24^2 \times 48$	1.23×10^{-8}
TDSLDA	240	Summit	442 368	$24^2 \times 48$	1.12×10^{-8}
TDSLDA-opt	240	Summit	442 368	$24^2 \times 48$	7.18×10^{-9}
TDSLDA-simp	2	Titan	684	$20^2 \times 60$	7.55×10^{-8}

amounts of data, we have taken advantage of fast input-output (I/O) methods and fast algorithms to exchange data between computing nodes. The detailed description of the approach and the code will be soon released [136].

APPENDIX B: SADDLE-TO-SCISSION TIMES

The saddle-to-scission times $\tau_{s\to s}$ extracted in this round of simulations is noticeably shorter than those extracted in our initial study [62]. Similar long scission-to-saddle times have been confirmed in Ref. [49] and even longer times (up to $\approx 3 \times 10^4$ fm/c) were reported in Ref. [86], in which a slight variation of the SLy4 NEDF, namely the SLy4d NEDF [137], was used. We attribute these differences partially to the difference of scalar effective masses between the energy functionals. Indeed, for SLy4 $m^* \approx 0.7m$, which is significantly smaller than $m^* = m$ for SeaLL1 and smaller than $m^* \approx 0.8m$ for SkyM*. One might argue that the SkM* effective mass is not much different from the SLy4 value. However, the Landau-Zener transition formula reads

$$P_{LZ} \approx \exp\left[-\frac{|\Delta|^2}{\hbar \dot{q} \varepsilon_q(q)}\right], \tag{B1}$$

where the energy difference between two adjacent sp levels $\varepsilon_q(q) \propto 1/m^*$ controls their relative slope with collective coordinate q. Since the effective mass also determines the sp level density, even a small difference can lead to large changes in P_{LZ}. Another source of differences arises from the treatment of the pairing correlations. Relatively large variations of the scission-to-saddle times were obtained in Ref. [62], depending on whether the pairing field had volume, surface, or mixed surface-volume character. The magnitude of the pairing gap is typically fixed from odd-even nuclear mass staggering and is thus insensitive to the magnitude of the effective mass, which controls the sp level density at the Fermi level and therefore the number of sp states actively taking part in forming the pairing condensate. In a nucleus with a smaller effective mass, the size of the pairing condensate is thus diminished when compared to the average sp level spacing. While SLy4 describes quite reasonably gross nuclear properties, the sp level density at the Fermi level is drastically reduced when compared to observations, which are consistent with an effective mass $m^* \approx m$. A smaller effective mass leads to a "choppier" potential energy landscape, which would inhibit the transitions at the Fermi level responsible for maintaining the sphericity of the local Fermi sphere; see Ref. [77] and Fig. 3.

APPENDIX C: IS COLLECTIVE FISSION DYNAMICS ADIABATIC?

The adiabatic approximation has been the bedrock of the microscopic theory of fission dynamics [27,28] (but not of all phenomenological models) for more than half a century. The statement which can be found even in well-established monographs [27,37] is that the collective motion is so slow that one can limit the collective energy to only quadratic terms. This leads to the next conclusion, that the microscopic treatment of fission dynamics can be based on the assumption that the collective motion can be almost fully decoupled from the intrinsic motion. However, this assumption has never been proven to be accurate in LACM of nuclei [39]. Ring and Schuck [37] note at the end of their Chapter 12, where the adiabatic time-dependent Hartree-Fock theory (ATDHF) is presented, that the assumption of adiabaticity is questionable.

Decoupling between collective and intrinsic DoF is equivalent to the assumption that while the collective degrees of freedom evolve in time, the intrinsics DoF remain unexcited [37] or in local thermal equilibrium in general. The only exception so far to this rule in literature is the full TDDFT [57,62], in which adiabaticity is not enforced. Adiabaticity of the collective motion, however, should not be conflated with the collective dynamics having a quasistatic character [138]. Collective motion can be very slow, while at the same time collective and intrinsic degrees DoF are fully coupled. Our main result is indeed that fission dynamics is most likely quasistatic in character but not adiabatic. The nuclear collective kinetic energy at scission is an order of magnitude smaller that the value the nucleus would have had in the case of an adiabatic evolution.

In a static description of the nuclear shape evolution, the sp levels display an up and down evolution, in a manner similar to the familiar Nilsson diagrams [37], and they experience many avoided level crossings. The nucleus will retain its

spherical local Fermi surface only if pairs of nucleons will be moved from the up-going levels to the down-going levels at these avoided crossings, as discussed in Sec. IV and Fig. 3. If such transitions do not occur with unit probability, the nucleus at a given nuclear shape will get excited and its local temperature and intrinsic entropy will increase. One might consider that a nucleus is described by a pure wave function (in the absence of coupling to photons or weak interactions), since the system made of a neutron impinging on a heavy nucleus (subsequently fissioning) is an isolated system. In that case, the von Neumann entropy is constant indeed

$$S_{\rm tot}(t) = -{\rm Tr}[\rho(t)\ln\rho(t)] \equiv 0, \quad \rho(t) = |\Psi(t)\rangle\langle\Psi(t)|, \tag{C1}$$

where the density matrix of the nucleus is $\rho(t) \equiv |\Psi(t)\rangle\langle\Psi(t)|$ and where $\Psi(t)$ is the exact many-body nuclear wave function at all times. However, what increases is the entanglement entropy of the intrinsic system

$$S_{\rm int}(t) = -{\rm Tr}_{\rm coll}[\rho(t)\ln\rho(t)] \geqslant 0, \tag{C2}$$

where the trace is taken only over the collective DoF, i.e., over the "nuclear shape" of the fissioning nucleus. As a result, also the intrinsic energy and the intrinsic temperature increase as well.

1. Adiabaticity and energy exchange

The intrinsic motion of the descending nucleus from the outer saddle toward the scission configuration is similar to the downward motion of a heavy railway car on a very steep hill with its wheels blocked. The wheels dot not rotate but slip and become extremely hot due to friction, since almost the entire gravitational potential energy of the railway car at the top of the hill is converted into heat and very little of it is converted into collective kinetic energy. In this case, the railway car velocity is equal to the terminal velocity. An object attains a terminal velocity when the conservative force is balanced by the friction force, the acceleration of the system effectively vanishes, and the inertia plays basically no role in its dynamics. The motion of the railway car is strongly nonadiabatic and the velocity of the railway car is slower than in the case of an adiabatic evolution. However, the motion is quasistatic.

For a typical actinide, the difference in the collective potential energy between the outer saddle and the scission configuration is ≈20 MeV. The conserved total energy of a nucleus can always be represented in TDDFT as

$$\begin{aligned} E_{\rm tot} &= E_{\rm coll}(t) + E_{\rm int}(t) \\ &\equiv \int d\mathbf{r}\frac{mn(\mathbf{r},t)\mathbf{v}^2(\mathbf{r},t)}{2} \\ &\quad + \int d\mathbf{r}\,\mathcal{E}(\tau(\mathbf{r},t) - n(\mathbf{r},t)m^2\mathbf{v}^2(\mathbf{r},t), n(\mathbf{r},t), ...), \end{aligned} \tag{C3}$$

where the local velocity is related to the local total momentum density $\mathbf{p}(\mathbf{r},t) = mn(\mathbf{r},t)\mathbf{v}(\mathbf{r},t)$. This decomposition is possible because the TDDFT energy density satisfies local Galilean invariance [57,108,109,139]. An estimate of the collective kinetic energy $E_{\rm coll}(t)$ can be obtained also within TDGCM and ATDHF theories from the solution of the Schrödinger equation for the collective wave function. As shown by Goeke and Reinhard [38] and discussed earlier by Peierls and Thouless [140], GCM with conjugate coordinates and ATDHF approaches are nearly identical.

If the adiabatic approximation were valid, $E_{\rm coll}(t)$ would be increasing while the nucleus descends from saddle to scission and would reach a value of ≈20 MeV. The collective velocity would reach a value $\mathbf{v}(\mathbf{r},t) \approx 0.01c$, which is small in comparison with the Fermi velocity $v_F \approx 0.25c$. In such a situation, the nucleus would remain cold at all times; it would follow the lowest potential energy surface, the intrinsic state would be a pure state, and the intrinsic entropy would be zero, since no irreversible energy transfer could occur between the intrinsic and collective DoF. The collective DoF would merely exert work on the intrinsic DoF. At the saddle point, the initial collective velocity would be zero, and the nucleus would accelerate in the descent from saddle to scission.

2. Overdamped evolution

Our results of the nuclear evolution from the saddle to scission, however, show that the nucleus experiences almost no acceleration: The collective inertia plays essentially no role in the dynamics. The collective flow energy never exceeds 1–2 MeV until the scission configuration is reached. This result is independent of initial conditions and NEDF used. The energy difference between the saddle and scission configurations is essentially entirely converted into intrinsic energy and never returns back to the collective degrees of freedom (DoF), which upon thermalization is converted into heat. Therefore, the intrinsic state of the nucleus is not a pure state anymore and the entropy of the intrinsic system naturally increases. The collective velocity is even smaller in magnitude now, $v_{\rm coll} \approx 0.002 \ldots 0.004c$. In spite of the fact that the collective velocity is now even smaller than in an ideal adiabatic evolution, the collective motion is not more "adiabatic." In thermodynamics, adiabatic processes conserve entropy and they should not be confused with quasistatic processes. Fission dynamics from the saddle to scission is a quasistatic process but not an adiabatic one. As discussed in Ref. [25], the inclusion of dissipation and fluctuations does not modify these conclusions.

Fission dynamics is thus similar to the overdamped motion of a Brownian particle [43,44]

$$m\ddot{\mathbf{q}}(t) = \mathbf{F}(\mathbf{q}(t)) - \overleftrightarrow{\gamma}\cdot\dot{\mathbf{q}}(t) + \mathbf{L}(t), \tag{C4}$$

when the acceleration $\ddot{\mathbf{q}}(t)$ vanishes this leads to

$$\overleftrightarrow{\gamma}\cdot\dot{\mathbf{q}}(t) = \mathbf{F}(\mathbf{q}(t)) + \mathbf{L}(t), \tag{C5}$$

where $\mathbf{F}(\mathbf{q}(t))$ is the conservative force, $\overleftrightarrow{\gamma}$ is the dissipation/friction tensor, and $\mathbf{L}(t)$ is a Langevin force. In the absence of fluctuations, a particle follows mainly the direction of the steepest descent

$$\dot{\mathbf{q}}(t) = \overleftrightarrow{\gamma}^{-1}\cdot\mathbf{F}(\mathbf{q}(t)) \tag{C6}$$

and inertia and acceleration becomes irrelevant. Even in the case of enhanced pairing correlations, the same kind of

dynamics emerges. In the presence of strong dissipation, one cannot describe the collective dynamics within a Hamiltonian approach.

3. Number of collective variables

The definition of collective coordinates is well known to be a problem with no satisfactory solution yet achieved in the microscopic theory of nuclear LACM [39]. Is it possible within GCM to introduce a parameter which characterizes the convergence of the expansion toward a physically accurate solution, particularly in the case of a nonequilibrium dynamics? Here we want to point to a few additional difficulties encountered while trying to introduce collective coordinates. One can ask if either TDGCM, ATDHF, or even the Langevin approach are controllable approximations. In particular, can one achieve a more accurate description and minimize theoretical errors by increasing the number of independent collective parameters? Naturally, not only the needed number of collective DoF is relevant but also their character. In the case of fission, one typically needs at least two DoF in the initial state, the quadrupole and octupole axial deformations, Q_{20} and Q_{30}. However, near the scission configuration, one needs to account for the separate quadrupole and octupole deformations of both incipient FFs; see Secs. V A and V D and Ref. [86]. These aspects indicate that from saddle to scission the number of physically relevant DoF is likely monotonically increasing.

If the nucleus is placed on a spatial lattice with $N_s = N_x N_y N_z$ lattice sites, clearly the number density cannot have more than N_s independent moments. Thus, in the GCM representation where generator coordinates are restricted to moments of the density, one cannot have more than N_s independent components. In our case, $N_s = 24^2 \times 48 = 27\,648$ and this would be the maximum number of independent collective coordinates possible. Can a fully correlated nuclear wave function be represented accurately as a sum over N_s Slater determinants? On a spatial lattice with $N_s = 27\,648$ lattice sites, the total number of possible Slater independent determinants for ^{240}Pu (with fixed N and Z) is

$$N_{\rm SD} = \frac{(2N_s)!}{Z!(2N_s - Z)!}\frac{(2N_s)!}{N!(2N_s - N)!} \approx 10^{739}, \tag{C7}$$

estimated by taking into account that at each spatial site one can place a nucleon with either spin up or down. While mathematically correct, this estimate is not necessarily physically correct, as most of these states are dynamically unreachable or physically irrelevant. However, this estimate proves the point that a set of Slater determinants parameterized by all possible shapes is incomplete and that raises the question of whether a GCM-like parametrization is ever accurate or under what conditions is accurate.

There was a proposal to increase the accuracy of GCM by including two quasiparticle excitations [141]. If a sufficient number of excitations would be introduced, one might hope that the total nucleus wave function is sufficiently accurate for describing fission. If sufficiently accurate, such a description could account for various fluctuations not accounted for in TDDFT. In the case of fission, one has to tackle the nonequilibrium dynamics of an open system described by the collective DoF, and the potential TDGCM representation of the total nucleus wave function would be

$$\Psi(\mathbf{x}, t) = \sum_k \int d\mathbf{q} f_k(\mathbf{q}, t)\Phi_k(\mathbf{x}|\mathbf{q}), \tag{C8}$$

where the summation over the index k includes both the ground state and the included many-quasiparticle excited states corresponding to a fixed shape $\mathbf{q}$. One typically assumes that a set of static generalized Slater determinants might be sufficient. The question, which has not been addressed by Bernard *et al.* [141], is the uniqueness of such a representation. In typical GCM implementations, the overlap matrix

$$\mathcal{N}(\mathbf{q}, \mathbf{q}') = \int d\mathbf{x}\Phi(\mathbf{x}|\mathbf{q})\Phi(\mathbf{x}|\mathbf{q}') \tag{C9}$$

has the majority of the eigenvalues either vanishing or very small, which is a result of the strong linear dependence of the basis set of generalized Slated determinants [40]. In the representation (C8), this aspect will obviously become even worse. A slight change in the shape of a nucleus can always be represented as a linear superposition of one quasiparticle excitations. A two-quasiparticle excitation can be viewed is as a part of a small nuclear shape change. Thus, introducing additional quasiparticle excitations into the GCM mix clearly leads to an additional linear dependence among the basis set of states.

One can easily convince oneself that even with this extension of the GCM, or even of the ATDHF method or Langevin approach for that matter, the number of independent time-dependent Slater determinants would still be much smaller than what is needed to obtain a complete representation of a total nuclear wave function. According to the calculations presented in Fig. 1, the number of proton and neutron one-quasiparticle states with an energy below 5 MeV is ≈140 and below 10 MeV in ^{240}Pu is ≈440, which would lead a prohibitively large number of components in such an extension. Moreover, it seems very unlikely that one could accurately represent excitation energies of the intrinsic system of ≈20 MeV with only two quasiparticle excitations added as additional collective coordinates. One might get a rough estimate by using statistical level densities [12,37],

$$\rho(N, Z, E^*) \propto (E^*)^{-5/4} \exp[2\sqrt{aE^*}], \tag{C10}$$

where E^* is the intrinsic excitation energy and $a \approx A/10$, or the combinatorial method [142,143]. Already at excitation energies corresponding to an incident thermal neutron on heavy nuclei, there are of the order of $O(10^6)$ [12–14] levels, and at 20 MeV excitation energy, one might expect $O(10^7)$ according to Eq. (C10). Therefore, one might rather safely infer that a GCM or an ATDHF representation of the total wave function of a nucleus at excitation energies ≈20 MeV would be numerically intractable, unless restricted to a few collective coordinates. Naturally, one may ask how many independent Slater determinants are needed to reach a given accuracy. This still remains an open question.

Some of the present authors believe that an improvement over current implementations of the TDGCM, ATDHF, and

Langevin approaches is the approach outlined in Ref. [25], in which all collective DoF are taken into account, plus dissipation and fluctuations, in a fully quantum extension of TDDFT. Would such an approach be theoretically sufficiently accurate? So far, the description of mass yields using various implementations of the Langevin approach [24,43–48] leads apparently in all cases to qualitatively similar results, in satisfactory agreement with experimental results. These results might simply point to the fact that these observables are relatively weakly sensitive to details of the Langevin approach implementation.

APPENDIX D: CRITIQUE OF THE STOCHASTIC MEAN-FIELD PRESCRIPTION

One can attempt to simulate the effect of a superposition of (generalized) Slater determinants suggested by the path-integral approach by following the stochastic mean-field model introduced by Ayik [87]. In the stochastic mean-field model, *fluctuations only stem from the fluctuations in the initial density* [49] and the time evolution is exactly the usual time-dependent mean field. This *ad hoc* assumption is at odds with the Langevin approach and also with the path-integral approach, in which fluctuations along the entire path are relevant.

One can easily check that in any classical Langevin description, if fluctuations vanish after a certain finite time, friction erases their memory in the long time limit. For example, if the force is constant, the solution of the classical Langevin equation is

$$m\dot{v}(t) = F - \gamma m v(t) + m\xi(t), \tag{D1}$$

$$v(t) = v(0)e^{-\gamma t} + \frac{F}{m\gamma}(1 - e^{-\gamma t}) + e^{-\gamma t}\int_0^t dt'\xi(t')e^{-\gamma t'}, \tag{D2}$$

the integral term becomes a constant, the role of fluctuations soon becomes exponentially small, and the particle continues moving with a constant terminal velocity.

The conclusion reached in Ref. [49] is at odds also with our quite firm conclusion that in nuclear LACM the memory of the initial conditions is washed out during the evolution rather quickly; see Secs. V A, V C, and V D. In our approach, we follow basically a similar strategy: The trajectories are obtained from a time-dependent mean-field dynamics. We chose our initial conditions from an ensemble of initial energies and initial collective variables with similar spreads. Because the one-body dissipation is so effective in bringing the collective flow almost to a stop, at any point on the potential energy surface the system will most likely follow the direction of the steepest descent, see Appendix B, and the collective inertia will have a marginal effect on the collective dynamics. Therefore, in its evolution from saddle to scission, the nucleus will largely follow the bottom of the fission valley. The collective nuclear motion becomes very similar to the motion of a viscous fluid.

Ayik's model is phenomenological in nature, like random matrix theory, since it involves simulating quantal fluctuations of observables with a random ensemble. This makes the statement of Tanimura *et al.* [49] that they obtained for the "first time a fully microscopic description of the fragment TKE distribution after fission" questionable.

We suggest that the discrepancies between the results of Ref. [49] and the path-integral approach, the Langevin approach, and our results too arise from the large unphysical fluctuations of all physical observables inherent to the stochastic mean-field approach, the nature of which we describe below. Since in the stochastic mean-field method *fluctuations only stem from the fluctuations in the initial density* [49] one would expect that their conclusions should parallel ours, as we have considered a relatively large set of initial conditions with a similar spread in initial energies and deformations.

In the stochastic mean-field prescription, one uses an ensemble $\{\lambda\}_{\lambda\in\Lambda}$ of one-body density matrices ρ^{λ}_{kl} such that

$$\rho^{\lambda}(\boldsymbol{r},\boldsymbol{r}',t) = \sum_{k,l}\phi_k(\boldsymbol{r},t)\rho^{\lambda}_{kl}\phi^*_l(\boldsymbol{r}',t), \tag{D3}$$

$$\rho^{\lambda}_{kl} = \rho^{\lambda *}_{lk} = n_k\delta_{kl} + \xi^{\lambda}_{kl}, \tag{D4}$$

$$i\hbar\dot{\phi}_k(\boldsymbol{r},t) = h[\rho^{\lambda}]\phi_k(\boldsymbol{r},t), \tag{D5}$$

where n_k are initial time-independent, zero-temperature, sp occupation probabilities obtained by considering pairing interactions and $\xi^{\lambda}_{kl} = \xi^{\lambda *}_{lk}$ are time-independent, independent Gaussian complex random numbers with zero mean and variance

$$\sigma^2_{kl} = \overline{\xi^{\lambda}_{kl}\xi^{\lambda *}_{kl}} = \tfrac{1}{2}[n_k(1-n_l) + n_l(1-n_k)], \tag{D6}$$

where the overline refers to statistical averaging over the events λ of the ensemble Λ. All other second moments of the distributions vanish. These Gaussian random numbers are chosen to be nonvanishing in a limited energy window around the Fermi level; see Fig. 13. By allowing these random fluctuations in the one-body density matrix, the total energy of the system also fluctuates. Both the intrinsic excitation energy of the nucleus and the size of the fluctuations of the total energy are controlled by the size of the sp energy window where fluctuations are nonvanishing.

A particularly illuminating example, which illustrates the difficulties of the stochastic mean field model, is the case of a single particle, when ($n_0 = 1,\ n_{k>0} = 0$)

$$\rho^{\lambda}(\boldsymbol{r},\boldsymbol{r}',t) = \phi_0(\boldsymbol{r},t)\phi^*_0(\boldsymbol{r}',t) + \sum_{k=1}^{M}\big[\xi^{\lambda}_{0k}\phi_0(\boldsymbol{r},t)\phi^*_k(\boldsymbol{r}',t) + \xi^{\lambda *}_{0k}\phi_k(\boldsymbol{r},t)\phi^*_0(\boldsymbol{r}',t)\big], \tag{D7}$$

$$\overline{\xi^{\lambda}_{0k}\xi^{\lambda *}_{0l}} = \frac{1}{2}\delta_{kl}, \quad \overline{\xi^{\lambda}_{0k}} = 0. \tag{D8}$$

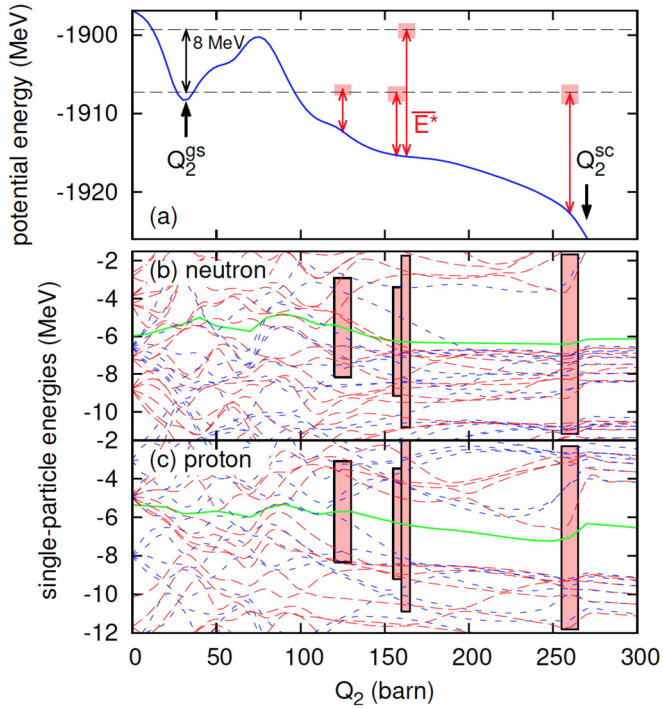

FIG. 13. Occupation probabilities of the nucleon levels within a window of approximately 5 MeV were prescribed random values as in Eqs. (D3), (D4), and (D6). The red bars show the size of the sp energy window, in the case of each deformation, where stochastic fluctuations are allowed. This is a copy of the Fig. 1 from the Supplemental Material of Ref. [49].

Simple algebraic manipulations show that the eigenvalue equation

$$\int d\mathbf{r}'\rho^{\lambda}(\boldsymbol{r},\boldsymbol{r}',t)\psi(\mathbf{r}',t) = \nu\psi(\mathbf{r},t) \tag{D9}$$

has two nonvanishing eigenvalues

$$\nu_{1,2} = \frac{1}{2} \pm \sqrt{\frac{1}{4} + \sum_{k=1}^{M} |\xi_k|^2} \approx \frac{1}{2} \pm \sqrt{\frac{1}{4} + \frac{M}{2}}, \tag{D10}$$

$$\lim_{M\to\infty} \nu_{1,2} = \pm\infty, \tag{D11}$$

even though $\nu_1 + \nu_2 \equiv 1$. Such a stochastic fermionic density matrix violates blatantly the Pauli principle. One can also show that

$$\begin{aligned}
&\int d\mathbf{r}''\rho^{\lambda}(\boldsymbol{r},\boldsymbol{r}'',t)\rho^{\lambda}(\boldsymbol{r}'',\boldsymbol{r}',t) \\
&= \rho^{\lambda}(\boldsymbol{r},\boldsymbol{r}',t) + \sum_{k=1}^{M} \phi_0(\mathbf{r},t)\xi_k^*\phi_k^*(\mathbf{r}',t) \\
&\quad + \sum_{k=1}^{M} \xi_k\phi_k(\mathbf{r}',t)\phi_0^*(\mathbf{r}',t) \\
&\quad + \phi_0(\mathbf{r},t)\phi_0^*(\mathbf{r}',t)\sum_{k=1}^{M}|\xi_k|^2 \\
&\quad + \sum_{k=1}^{M}\xi_k\phi_k(\mathbf{r},t)\sum_{l=1}^{M}\xi_l^*\phi_l^*(\mathbf{r}',t),
\end{aligned} \tag{D12}$$

$$\overline{\mathrm{Tr}\rho^{\lambda}} = 0, \quad \overline{\mathrm{Tr}[\rho^{\lambda}]^2} = 1 + M, \quad \lim_{M\to\infty} \mathrm{Tr}[\rho^{\lambda}]^2 = \infty. \tag{D13}$$

Even though the particle number is conserved on average in the stochastic mean-field approach, the variance of the particle number is extremely large or even infinite if the entire sp spectrum is included. These higher moments enter into the expressions of the total energy and the sp Hamiltonian.

For an arbitrary number of particles, the Hermitian matrix $n_k\delta_{kl} + \xi_{kl}^{\lambda} = \sum_m S_{km}^{\lambda}\nu_m^{\lambda}S_{lm}^{\lambda *}$ can be diagonalized and the density matrix can be rewritten as

$$\rho^{\lambda}(\boldsymbol{r},\boldsymbol{r}',t) = \sum_m \psi_m^{\lambda}(\boldsymbol{r},t)\nu_m^{\lambda}\psi_m^{\lambda *}(\boldsymbol{r}',t), \tag{D14}$$

where $\psi_k^{\lambda}(\boldsymbol{r},t) = \sum_l \phi_l(\boldsymbol{r},t)S_{lk}^{\lambda}$ and $\sum_m S_{km}^{\lambda}S_{lm}^{\lambda *} = \delta_{kl}$. Both sets of sp wave functions in Eq. (D3) or in the equivalent Eq. (D14) satisfy the same TDHF equations (D4) with the sp Hamiltonian $h[\rho^{\lambda}]$ defined through the random density matrix $\rho^{\lambda}(\boldsymbol{r},\boldsymbol{r}',t)$, Eq. (D3).

In Figs. 14 and 15, we illustrate the problems with the stochastic mean-field prescription, which leads to effective occupation probabilities ν_m^{λ} outside the physical interval [0, 1], which is a flagrant violation of the Pauli principle. The statistical average value of the particle number is correct:

$$\overline{\langle\hat{N}\rangle} = \overline{\mathrm{tr}\rho^{\lambda}} = \sum_k \overline{n_k + \xi_{kk}^{\lambda}} = \sum_k n_k. \tag{D15}$$

However, since the fluctuations are very large (even infinite if the entire spectrum is included), the total energy

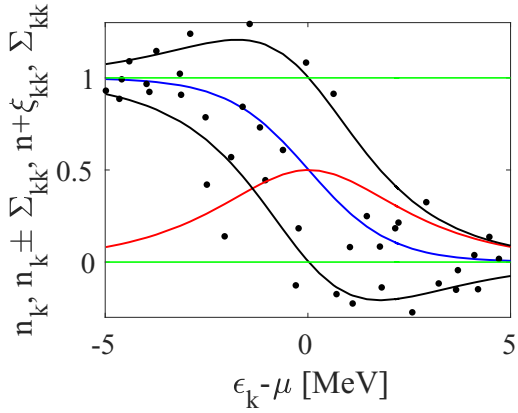

FIG. 14. Average neutron occupation probabilities n_k (blue) for a system with $N = 150$, a Fermi energy $\varepsilon_F = 35$ MeV, and an almost constant average sp level density at a temperature 1 MeV, the $\rho_{kk} = n_k \pm \sigma_{kk}$ (black) and σ_{kk} (red), and a typical random realization of the stochastic occupation probabilities $n_k + \xi_{kk}$ (black dots) chosen in an energy window $(-5, 5)$ MeV around the Fermi level.

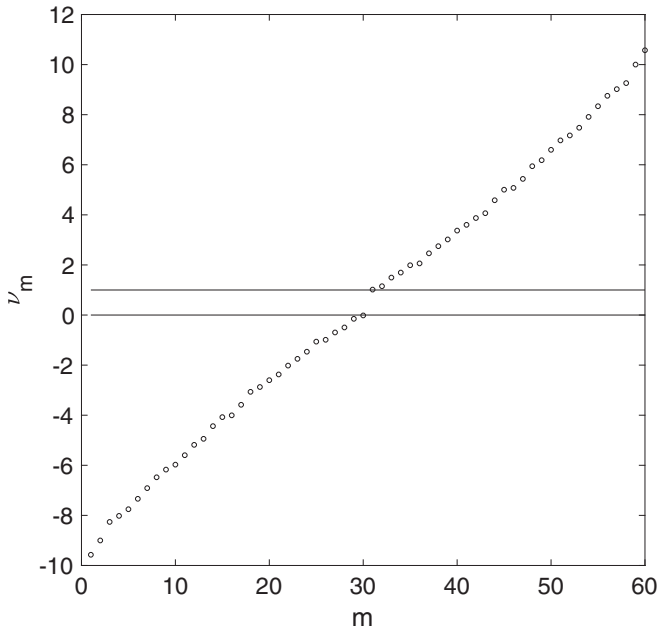

FIG. 15. The "occupation probabilities" ν_m (D14) after the diagonalization of one stochastic realization of Eq. (D4) for $n_{k=1...30} = 1$ and $n_{l=31...60} = 0$. Two horizontal lines are at 0 and 1 levels. The shape of this spectrum of the "occupation probabilities" changes little from one stochastic realization to another. The range of ν_m values increases with the size of the energy interval over which fluctuations are allowed, covering the entire real axis, if the fluctuations are allowed over the entire sp spectrum.

of the nucleus has also very large unphysical fluctuations. Let us estimate now the statistical average of a typical interaction term

$$\int d\boldsymbol{r}\overline{\rho^2(\boldsymbol{r},\boldsymbol{r},t)}$$
$$= \int d\boldsymbol{r}\left[\sum_k n_k|\phi_k(\boldsymbol{r},t)|^2\right]^2$$
$$+ \frac{1}{2}\int d\boldsymbol{r}\sum_{kl}|\phi_k(\boldsymbol{r},t)|^2|\phi_l(\boldsymbol{r},t)|^2[n_k + n_l - 2n_k n_l]$$
$$= \int d\boldsymbol{r}\sum_{kl} n_k|\phi_k(\boldsymbol{r},t)|^2|\phi_l(\boldsymbol{r},t)|^2$$
$$\approx \frac{NN_{\rm lev}}{V}, \tag{D16}$$

where we have considered for the sake of simplicity of the argument only the sp states in the window where fluctuations are allowed. V is the volume of the system. This can be very different from the real value,

$$\int d\boldsymbol{r}\rho^2(\boldsymbol{r},\boldsymbol{r},t) \approx N\frac{N}{V} \ll N_{\rm lev}\frac{N}{V}. \tag{D17}$$

In Ref. [49], the authors use the parameter $N_{\rm lev} > N$ to control by how much they can affect the internal energy of the nucleus. A simpler and equally arbitrary approach would be to multiply the density $\rho(\boldsymbol{r},\boldsymbol{r},t)$ by $1+\xi$, where ξ is a random number with zero mean. The size of the fluctuations of the energy of the nucleus is controlled in Ref. [49] by the arbitrary number of the sp levels $N_{\rm lev}$, or by the arbitrary size of the sp energy window where such fluctuations are allowed. As a result, the unphysical particle fluctuations lead also to unphysical energy fluctuations in the stochastic mean-field approach.

There is no theoretical argument presented in Ref. [49] on how to choose the starting point of the dynamical simulations. For $Q_{20} > 125$ barn, as is clearly seen from Fig. 13, the FFs have been already well individualized and no redistribution of the sp occupation numbers occurs anymore. At these deformations, the size of this sp energy window is chosen so as to reproduce on average the increase in the total energy of the nucleus to match the ground-state energy. It would seem more natural to start the simulation at the exact configuration where the nucleus emerged from under the barrier at $Q_{20} \approx 100$ barn. In that case, the size of the "fluctuations" would be zero, as the nucleus emerges from under the barrier in its intrinsic ground state. Starting at the deformation $Q_{20} \approx 100$ barn, however, would deprive the authors of the ability to generate a desired FF distribution, induced by the presence of fluctuations. The authors even establish that if they were to start their simulations closer to the scission configurations their results would be quite different, thus precluding this approach of its predictive power. One can thus safely conclude that the FF distributions definitely depend strongly on the choice of the initial conditions within such a stochastic mean-field approach.

[1] O. Hahn and F. Strassmann, Über den Nachweis und das Verhalten der bei der Bestrahlung des Urans mittels Neutronen entstehenden Erdalkalimetalle, Naturwissenschaften **27**, 11 (1939).
[2] L. Meitner and O. R. Frisch, Disintegration of uranium by neutrons: A new type of nuclear reaction, Nature (London) **143**, 239 (1939).
[3] T. J. Jorgensen, Lise Meitner—the forgotten woman of nuclear physics who deserved a Nobel Prize, https://theconversation.com.
[4] I. Noddack, Uber das Element 93, Z. Angew. Chem. **47**, 653 (1934).
[5] E. Fermi, Possible production of elements of atomic number higher than 92, Nature (London) **133**, 898 (1934).
[6] E. Fermi, Radioactivity induced by neutron bombardment, Nature (London) **133**, 757 (1934).
[7] J. M. Pearson, On the belated discovery of fission, Phys. Today **68**(6), 40 (2015).
[8] G. Gamow, Mass defect curve and nuclear constitution, Proc. R. Soc. London, Ser. A **126**, 632 (1930).
[9] R. Stuewer, An act of creation: The Meitner-Frisch interpretation of nuclear fission, http://edition-open-access.de/proceedings/5/11/index.html.

[10] N. Bohr and J. A. Wheeler, The mechanism of nuclear fission, Phys. Rev. **56**, 426 (1939).

[11] N. Bohr, Neutron capture and nuclear constitution, Nature (London) **137**, 344 (1936).

[12] A. Bohr and B. R. Mottelson, *Nuclear Structure*, Vol. I (Benjamin, New York, 1969).

[13] R. Capote, M. Herman, P. Obložinský, P. G. Young, S. Goriely, T. Belgya, A. V. Ignatyuk, A. J. Koning, S. Hilaire, V. A. Plujko *et al.*, RIPL—Reference Input Parameter Library for calculation of nuclear reactions and nuclear data evaluations, Nucl. Data Sheets **110**, 3107 (2009).

[14] T. von Egidy and D. Bucurescu, Systematics of nuclear level density parameters, Phys. Rev. C **72**, 044311 (2005).

[15] V. Weisskopf, Statistics and nuclear reactions, Phys. Rev. **52**, 295 (1937).

[16] W. Hauser and H. Feshbach, The inelastic scattering of neutrons, Phys. Rev. **87**, 366 (1952).

[17] V. M. Strutinsky, Shell effects in nuclear masses and deformation energies, Nucl. Phys. A **95**, 420 (1967).

[18] M. Brack, J. Damgaard, A. S. Jensen, H. C. Pauli, V. M. Strutinsky, and C. Y. Wong, Funny Hills: The shell-correction approach to nuclear shell effects and its applications to the fission process, Rev. Mod. Phys. **44**, 320 (1972).

[19] S. Bjornholm and J. E. Lynn, The double-humped fission barrier, Rev. Mod. Phys. **52**, 725 (1980).

[20] J. W. Negele and H. Orland, *Quantum Many-Particle Systems* (Westview Press, Reading, MA, 1998).

[21] A. Bulgac, The long journey from *ab initio* calculations to density functional theory for nuclear large amplitude collective motion, J. Phys. G: Nucl. Part. Phys. **37**, 064006 (2010).

[22] D. L. Hill and J. A. Wheeler, Nuclear constitution and the interpretation of fission phenomena, Phys. Rev. **89**, 1102 (1953).

[23] J. J. Griffin and J. A. Wheeler, Collective motions in nuclei by the method of generator coordinates, Phys. Rev. **108**, 311 (1957).

[24] P. Fröbrich and I. I. Gontchar, Langevin description of fusion, deep-inelastic collisions, and heavy-ion-induced fission, Phys. Rep. **292**, 131 (1998).

[25] A. Bulgac, S. Jin, and I. Stetcu, Unitary evolution with fluctuations and dissipation, Phys. Rev. C **100**, 014615 (2019).

[26] J. Blocki, Y. Boneh, J. R. Nix, J. Randrup, M. Robel, A. J. Sierk, and W. J. Swiatecki, One-body dissipation and the super-viscidity of nuclei, Ann. Phys. **113**, 330 (1978).

[27] J. K. Krappe and K. Pomorski, *Theory of Nuclear Fission* (Springer, Heidelberg, 2012).

[28] N. Schunck and L. M. Robledo, Microscopic theory of nuclear fission: A review, Rep. Prog. Phys. **79**, 116301 (2016).

[29] H. Goutte, J. F. Berger, P. Casoli, and D. Gogny, Microscopic approach of fission dynamics applied to fragment kinetic energy and mass distributions in ^{238}U, Phys. Rev. C **71**, 024316 (2005).

[30] D. Regnier, N. Dubray, N. Schunck, and M. Verrière, Fission fragment charge and mass distributions in ^{239}Pu(n, f) in the adiabatic nuclear energy density functional theory, Phys. Rev. C **93**, 054611 (2016).

[31] A. Zdeb, A. Dobrowolski, and M. Warda, Fission dynamics of ^{252}Cf, Phys. Rev. C **95**, 054608 (2017).

[32] N. Schunck, editor, *Energy Density Functional Methods for Atomic Nuclei* (IOP Publishing, Bristol, UK, 2019).

[33] W. Younes, D. M. Gogny, and J. F. Berger, *A Microscopic Theory of Fission Dynamics Based on the Generator Coordinate Method*, Lectures Notes in Physics Vol. 950 (Springer, Berlin, 2019).

[34] M. Baranger, Microscopic view of nuclear collective properties, J. Phys. **33**, C5 (1972).

[35] M. Baranger and M. Véneroni, An adiabatic time-dependent Hartree-Fock theory of collective motion in finite systems, Ann. Phys. **114**, 123 (1978).

[36] F. Villars, Adiabatic time-dependent Hartree-Fock theory in nuclear physics, Nucl. Phys. A **285**, 269 (1978).

[37] P. Ring and P. Schuck, *The Nuclear Many-Body Problem*, Theoretical and Mathematical Physics Series No. 17 (Springer-Verlag, Berlin, 2004).

[38] K. Goeke and P.-G. Reinhard, The generator-coordinate-method with conjugate parameters and the unification of microscopic theories for large amplitude collective motion, Ann. Phys. **124**, 249 (1980).

[39] G.-D. Dang, A. Klein, and N. R. Walet, Self-consistent theory of large-amplitude collective motion: Applications to approximate quantization of nonseparable systems and to nuclear physics, Phys. Rep. **335**, 93 (2000).

[40] G. Bertsch and H. Flocard, Pairing effects in nuclear collective motion: Generator coordinate method, Phys. Rev. C **43**, 2200 (1991).

[41] N. W. Aschroft and N. D. Mermin, *Solid State Physics* (Saunders College, Philadelphia, 1976).

[42] P. Möller, D. G. Madland, A. J. Sierk, and A. Iwamoto, Nuclear fission modes and fragment mass asymmetries in a five-dimensional deformation space, Nature (London) **409**, 785 (2001).

[43] J. Randrup and P. Möller, Brownian Shape Motion on Five-Dimensional Potential-Energy Surfaces: Nuclear Fission-Fragment Mass Distributions, Phys. Rev. Lett. **106**, 132503 (2011).

[44] J. Randrup, P. Möller, and A. J. Sierk, Fission-fragment mass distributions from strongly damped shape evolution, Phys. Rev. C **84**, 034613 (2011).

[45] A. J. Sierk, Langevin model of low-energy fission, Phys. Rev. C **96**, 034603 (2017).

[46] C. Ishizuka, M. D. Usang, F. A. Ivanyuk, J. A. Maruhn, K. Nishio, and S. Chiba, Four-dimensional Langevin approach to low-energy nuclear fission of ^{236}U, Phys. Rev. C **96**, 064616 (2017).

[47] J. Sadhukhan, W. Nazarewicz, and N. Schunck, Microscopic modeling of mass and charge distributions in the spontaneous fission of ^{240}Pu, Phys. Rev. C **93**, 011304(R) (2016).

[48] J. Sadhukhan, C. Zhang, W. Nazarewicz, and N. Schunck, Formation and distribution of fragments in the spontaneous fission of ^{240}Pu, Phys. Rev. C **96**, 061301(R) (2017).

[49] Y. Tanimura, D. Lacroix, and S. Ayik, Microscopic Phase-Space Exploration Modeling of ^{258}Fm Spontaneous Fission, Phys. Rev. Lett. **118**, 152501 (2017).

[50] B. D. Wilkins and E. P. Steinberg, Semi-empirical interpretation of nuclear fission based on deformed-shell effects, Phys. Lett. B **42**, 141 (1972).

[51] B. D. Wilkins, E. P. Steinberg, and R. R. Chasman, Scission-point model of nuclear fission based on deformed-shell effects, Phys. Rev. C **14**, 1832 (1976).

[52] J.-F. Lemaître, S. Panebianco, J.-L. Sida, S. Hilaire, and S. Heinrich, New statistical scission-point model to predict fission fragment observables, Phys. Rev. C **92**, 034617 (2015).

[53] J. Randrup and P. Möller, Energy dependence of fission-fragment mass distributions from strongly damped shape evolution, Phys. Rev. C **88**, 064606 (2013).
[54] D. E. Ward, B. G. Carlsson, T. Døssing, P. Möller, J. Randrup, and S. Åberg, Nuclear shape evolution based on microscopic level densities, Phys. Rev. C **95**, 024618 (2017).
[55] M. Albertsson, B. G. Carlsson, T. Døssing, P. Møller, J. Randrup, and S. Åberg, Microscopic treatment of energy partition in fission, arXiv:1811.02283.
[56] A. Bulgac, M. M. Forbes, and P. Magierski, The unitary Fermi gas: From Monte Carlo to density functionals, in *The BCS–BEC Crossover and the Unitary Fermi Gas*, edited by W. Zwerger, Lecture Notes in Physics Vol. 836 (Springer-Verlag, Berlin, 2012), Chap. 9, pp. 127–191.
[57] A. Bulgac, Time-dependent density functional theory and the real-time dynamics of Fermi superfluids, Ann. Rev. Nucl. Part. Sci. **63**, 97 (2013).
[58] A. Bulgac, Time-dependent density functional theory for fermionic superfluids: From cold atomic gases, to nuclei and neutron star crust, Phys. Status Solidi B **256**, 1800592 (2019).
[59] S. Jin, A. Bulgac, K. Roche, and G. Wlazłowski, Coordinate-space solver for superfluid many-fermion systems with the shifted conjugate-orthogonal conjugate-gradient method, Phys. Rev. C **95**, 044302 (2017).
[60] A. Bulgac and M. McNeil Forbes, Use of the discrete variable representation basis in nuclear physics, Phys. Rev. C **87**, 051301(R) (2013).
[61] R. Navarro Perez, N. Schunck, R.-D. Lasseri, C. Zhang, and J. Sarich, Axially deformed solution of the Skyrme-Hartree-Fock-Bogolyubov equations using the transformed harmonic oscillator basis (III) hfbtho (v3.00): A new version of the program, Comput. Phys. Commun. **220**, 363 (2017).
[62] A. Bulgac, P. Magierski, K. J. Roche, and I. Stetcu, Induced Fission of ^{240}Pu Within a Real-Time Microscopic Framework, Phys. Rev. Lett. **116**, 122504 (2016).
[63] E. Chabanat, P. Bonche, P. Haensel, J. Meyer, and R. Schaeffer, A Skyrme parametrization from subnuclear to neutron star densities, part II. Nuclei far from stabilities, Nucl. Phys. A **635**, 231 (1998).
[64] P. Moller, J. R. Nix, W. D. Myers, and W. J. Swiatecki, Nuclear ground-state masses and deformations, At. Data Nucl. Data Tables **59**, 185 (1995).
[65] P. Möller, A. J. Sierk, and A. Iwamoto, Five-Dimensional Fission-Barrier Calculations from ^{70}Se to ^{252}Cf, Phys. Rev. Lett. **92**, 072501 (2004).
[66] P. Möller, A. J. Sierk, T. Ichikawa, A. Iwamoto, R. Bengtsson, H. Uhrenholt, and S. Åberg, Heavy-element fission barriers, Phys. Rev. C **79**, 064304 (2009).
[67] P. Möller, W. D. Myers, H. Sagawa, and S. Yoshida, New Finite-Range Droplet Mass Model and Equation-of-State Parameters, Phys. Rev. Lett. **108**, 052501 (2012).
[68] M. Dutra, O. Lourenço, J. S. Sá Martins, A. Delfino, J. R. Stone, and P. D. Stevenson, Skyrme interaction and nuclear matter constraints, Phys. Rev. C **85**, 035201 (2012).
[69] J. Bartel, P. Quentin, M. Brack, C. Guet, and H.-B. Håkansson, Towards a better parametrisation of Skyrme-like effective forces: A critical study of the SkM force, Nucl. Phys. A **386**, 79 (1982).
[70] M. Kortelainen, J. McDonnell, W. Nazarewicz, P.-G. Reinhard, J. Sarich, N. Schunck, M. V. Stoitsov, and S. M. Wild, Nuclear energy density optimization: Large deformations, Phys. Rev. C **85**, 024304 (2012).
[71] A. Bulgac, M. McNeil Forbes, S. Jin, R. N. Perez, and N. Schunck, Minimal nuclear energy density functional, Phys. Rev. C **97**, 044313 (2018).
[72] N. Schunck, D. Duke, H. Carr, and A. Knoll, Description of induced nuclear fission with Skyrme energy functionals: Static potential energy surfaces and fission fragment properties, Phys. Rev. C **90**, 054305 (2014).
[73] M. Bender, P.-H. Heenen, and P. Bonche, Microscopic study of ^{240}Pu: Mean field and beyond, Phys. Rev. C **70**, 054304 (2004).
[74] M. Kortelainen, J. McDonnell, W. Nazarewicz, E. Olsen, P.-G. Reinhard, J. Sarich, N. Schunck, S. M. Wild, D. Davesne, J. Erler, and A. Pastore, Nuclear energy density optimization: Shell structure, Phys. Rev. C **89**, 054314 (2014).
[75] J. F. Berger, M. Girod, and D. Gogny, Constrained Hartree-Fock and beyond, Nucl. Phys. A **502**, 85 (1989).
[76] R. Jodon, M. Bender, K. Bennaceur, and J. Meyer, Constraining the surface properties of effective Skyrme interactions, Phys. Rev. C **94**, 024335 (2016).
[77] G. Bertsch, The nuclear density of states in the space of nuclear shapes, Phys. Lett. B **95**, 157 (1980).
[78] F. Barranco, G. F. Bertsch, R. A. Broglia, and E. Vigezzi, Large-amplitude motion in superfluid Fermi droplets, Nucl. Data Sheet Phys. A **512**, 253 (1990).
[79] G. F. Bertsch and A. Bulgac, Comment on "Spontaneous Fission: A Kinetic Approach", Phys. Rev. Lett. **79**, 3539 (1997).
[80] G. F. Bertsch, W. Younes, and L. M. Robledo, Scission dynamics with k partitions, Phys. Rev. C **97**, 064619 (2018).
[81] Y. Tanimura, D. Lacroix, and G. Scamps, Collective aspects deduced from time-dependent microscopic mean-field with pairing: Application to the fission process, Phys. Rev. C **92**, 034601 (2015).
[82] P. Goddard, P. Stevenson, and A. Rios, Fission dynamics within time-dependent Hartree-Fock: Deformation-induced fission, Phys. Rev. C **92**, 054610 (2015).
[83] P. Goddard, P. Stevenson, and A. Rios, Fission dynamics within time-dependent Hartree-Fock. II. Boost-induced fission, Phys. Rev. C **93**, 014620 (2016).
[84] A. Bulgac and S. Jin, Dynamics of Fragmented Condensates and Macroscopic Entanglement, Phys. Rev. Lett. **119**, 052501 (2017).
[85] G. Scamps and Y. Hashimoto, Density-constraint time-dependent Hartree-Fock-Bogoliubov method, Phys. Rev. C **100**, 024623 (2019).
[86] C. Simenel and G. Scamps, Impact of pear-shaped fission fragments on mass-asymmetric fission in actinides, Nature (London) **564**, 382 (2018).
[87] S. Ayik, A stochastic mean-field approach for nuclear dynamics, Phys. Lett. B **658**, 174 (2008).
[88] C. Wagemans, E. Allaert, A. Deruytter, R. Barthélémy, and P. Schillebeeckx, Comparison of the energy and mass characteristics of the Pu239(nth,f) and the Pu240(sf) fragments, Phys. Rev. C **30**, 218 (1984).
[89] P. Schillebeeckx, C. Wagemans, A. J. Deruytter, and R. Barthélémy, Comparative study of the fragments' mass and energy characteristics in the spontaneous fussion of ^{238}Pu, ^{240}Pu and ^{242}Pu and in the thermal-neutron-induced fission of ^{239}Pu, Nucl. Phys. A **545**, 623 (1992).

[90] A. C. Wahl, Systematics of Fission-Product Yields, Tech. Rep. LA-13928, Los Alamos, NM, 2002 (unpublished).

[91] R. Vogt, J. Randrup, J. Pruet, and W. Younes, Event-by-event study of prompt neutrons from ^{239}Pu(n, f), Phys. Rev. C **80**, 044611 (2009).

[92] D.G. Madland, Total prompt energy release in the neutron-induced fission of ^{235}U, ^{238}U, and ^{239}Pu, Nucl. Phys. A **772**, 113 (2006).

[93] P. Talou, B. Becker, T. Kawano, M. B. Chadwick, and Y. Danon, Advanced Monte Carlo modeling of prompt fission neutrons for thermal and fast neutron-induced fission reactions on ^{239}Pu, Phys. Rev. C **83**, 064612 (2011).

[94] B. Becker, P. Talou, T. Kawano, Y. Danon, and I. Stetcu, Monte Carlo Hauser-Feshbach predictions of prompt fission γ rays: Application to $n_{\rm th} + ^{235}$U, $n_{\rm th} + ^{239}$Pu, and ^{252}Cf (sf), Phys. Rev. C **87**, 014617 (2013).

[95] J. M. Verbeke, J. Randrup, and R. Vogt, Fission reaction event yield algorithm, FREYA—For event-by-event simulation of fission, Comput. Phys. Commun. **191**, 178 (2015).

[96] J. M. Verbeke, J. Randrup, and R. Vogt, Fission reaction event yield algorithm FREYA 2.0.2, Comput. Phys. Commun. **222**, 263 (2018).

[97] N. Schunck, D. Duke, and H. Carr, Description of induced nuclear fission with Skyrme energy functionals. II. Finite temperature effects, Phys. Rev. C **91**, 034327 (2015).

[98] G. Audi, M. Wang, A. H. Wapstra, F. G. Kondev, M. MacCormick, X. Xu, and B. Pfeiffer, The AME2012 atomic mass evaluation, Chin. Phys. C **36**, 1287 (2012).

[99] V. F. Apalin, Y. N. Gritsyuk, I. E. Kutikov, V. I. Lebedev, and L. A. Mikaelian, Neutron emission from U233, U235, and Pu239 fission fragments, Nucl. Phys. **71**, 553 (1965).

[100] K. Nishio, Y. Nakagome, H. Yamamoto, and I. Kimura, Multiplicity and energy of neutrons from ^{235}U(n_{th}, f) fission fragments, Nucl. Phys. A **632**, 540 (1998).

[101] C. Tsuchiya, Y. Nakagome, H. Yamana, H. Moriyama, K. Nishio, I. Kanno, K. Shin, and I. Kimura, Simultaneous measurement of prompt neutrons and fission fragments for 239Pu(nth,f), J. Nucl. Sci. Tech. **37**, 941 (2000).

[102] O. A. Batenkov, G. A. Boykov, F.-J. Hambsch, J. H. Hamilton, V. A. Jakovlev, V. A. Kalinin, A. B. Laptev, V. E. Sokolov, and A. S. Vorobyev, in *International Conference on Nuclear Data for Science and Technology*, edited by R. C. Haight, M. B. Chadwick, T. Kawano, and P. Talou, AIP Conf. Proc. No. 769 (AIP, New York, 2005), p. 1003.

[103] I. Stetcu, P. Talou, and T. Kawano, Neutron-induced fission: Properties of prompt neutron and γ rays as a function of incident energy, EPJ Web Conf. **122**, 01012 (2016).

[104] R. Müller, A. A. Naqvi, F. Käppeler, and F. Dickmann, Fragment velocities, energies, and masses from fast neutron induced fission of ^{235}U, Phys. Rev. C **29**, 885 (1984).

[105] A. A. Naqvi, F. Käppeler, F. Dickmann, and R. Müller, Fission fragment properties in fast-neutron-induced fission of ^{237}Np, Phys. Rev. C **34**, 218 (1986).

[106] E. A. Uehling and G. E. Uhlenbeck, Transport phenomena in Einstein-Bose and Fermi-Dirac gases. I, Phys. Rev. **43**, 552 (1933).

[107] G. F. Bertsch and S. Das Gupta, A guide to microscopic models for intermediate energy heavy ion collisions, Phys. Rep. **160**, 189 (1988).

[108] Y. M. Engel, D. M. Brink, K. Goeke, S. J. Krieger, and D. Vautherin, Time-dependent Hartree-Fock theory with Skyrme's interaction, Nucl. Phys. A **249**, 215 (1975).

[109] M. Bender, P.-H. Heenen, and P.-G. Reinhard, Self-consistent mean-field models for nuclear structure, Rev. Mod. Phys. **75**, 121 (2003).

[110] R. Capote, N. Carjan, and S. Chiba, Scission neutrons for U, Pu, Cm, and Cf isotopes: Relative multiplicities calculated in the sudden limit, Phys. Rev. C **93**, 024609 (2016).

[111] N. Carjan and M. Rizea, Structures in the energy distribution of the scission neutrons: Finite neutron-number effect, Phys. Rev. C **99**, 034613 (2019).

[112] A. S. Vorobyev, O. A. Shcherbakov, A. M. Gagarski, G. V.Val'ski, and G. A. Petrov, Investigation of the prompt neutron emission mechanism in low energy fission of ^{235,233}U$(n_{th}\, f)$ and ^{252}Cf(sf), EPJ Web Conf. **8**, 03004 (2010).

[113] N. V. Kornilov, A. B. Kagalenko, S. V. Poupko, P. A. Androsenko, and F.-J. Hambsch, New evidence of an intense scission neutron source in the ^{252}Cf spontaneous fission, Nucl. Phys. A **686**, 187 (2001).

[114] N. V. Kornilov, A. B. Kagalenko, and F.-J. Hambsch, Prescission neutrons in the fission of ^{235}U and ^{252}Cf nuclei, Phys. Atom. Nucl. **64**, 1373 (2001).

[115] G. A. Petrov, in *Nuclear Fission and Fission-Product Spectroscopy: 3rd International Workshop on Nuclear Fission and Fission-Product Spectroscopy*, edited by H. Goutte, H. Faust, G. Fioni, and D. Goutte, AIP Conf. Proc. No. 798 (AIP, New York, 2005), p. 205.

[116] P. A. Anderson, *Basic Notions of Condensed Matter Physics* (Benjamin/Cummins, London, 1984).

[117] J. Dechargé and D. Gogny, Hartree-Fock-Bogolyubov calculations with the $D1$ effective interaction on spherical nuclei, Phys. Rev. C **21**, 1568 (1980).

[118] T. Ledergerbert, Z. Paltiel, Z. Fraenkel, and H. C. Pauli, Dynamic excitation in fission, Nucl. Phys. A **275**, 280 (1977).

[119] E. Fermi, On the origin of the cosmic radiation, Phys. Rev. **75**, 1169 (1949).

[120] J. W. Negele, S. E. Koonin, P. Möller, J. R. Nix, and A. J. Sierk, Dynamics of induced fission, Phys. Rev. C **17**, 1098 (1978).

[121] D. Regnier, N. Dubray, and N. Schunck, From asymmetric to symmetric fission in the fermium isotopes within the time-dependent generator-coordinate-method formalism, Phys. Rev. C **99**, 024611 (2019).

[122] G. F. Bertsch, T. Kawano, and L. M. Robledo, Angular momentum of fission fragments, Phys. Rev. C **99**, 034603 (2019).

[123] A. Bulgac, Projection of good quantum numbers for reaction fragments, Phys. Rev. C **100**, 034612 (2019).

[124] J. Grineviciute, P. Magierski, A. Bulgac, S. Jin, and I. Stetcu, Accuracy of fission dynamics within the time-dependent superfluid local density approximation, Acta Phys. Pol. **49**, 591 (2018).

[125] I. Stetcu, C. Bertulani, A. Bulgac, P. Magierski, and K. J. Roche, Relativistic Coulomb Excitation Within Time-Dependent Superfluid Local Density Approximation, Phys. Rev. Lett. **114**, 012701 (2015).

[126] W. Ryssens, P.-H. Heenen, and M. Bender, Numerical accuracy of mean-field calculations in coordinate space, Phys. Rev. C **92**, 064318 (2015).

[127] A. Castro, A. Rubio, and M. J. Stott, Solution of Poisson's equation for finite systems using plane wave methods, Can. J. Phys. **81**, 1151 (2003).

[128] D. Vautherin, Hartree-Fock calculations with Skyrme's interaction. II. Axially deformed nuclei, Phys. Rev. C **7**, 296 (1973).

[129] M. V. Stoitsov, J. Dobaczewski, W. Nazarewicz, and P. Ring, Axially deformed solution of the Skyrme-Hartree-Fock-Bogolyubov equations using the transformed harmonic oscillator basis: The program HFBTHO (v1.66p), Comput. Phys. Commun. **167**, 43 (2005).

[130] Y. Castin and F. Werner, The unitary Fermi gas and its symmetry properties, in *The BCS–BEC Crossover and the Unitary Fermi Gas*, Lecture Notes in Physics Vol. 836, edited by W. Zwerger (Springer-Verlag, Berlin, 2012), Chap. 5, pp. 127–191.

[131] A. Bulgac and Y. Yu, Renormalization of the Hartree-Fock-Bogoliubov Equations in the Case of a Zero Range Pairing Interaction, Phys. Rev. Lett. **88**, 042504 (2002).

[132] Y. Yu and A. Bulgac, Energy Density Functional Approach to Superfluid Nuclei, Phys. Rev. Lett. **90**, 222501 (2003).

[133] R. W. Hamming, *Numerical Methods for Scientists and Engineers* (Dover, New York, 1986).

[134] J. A. Maruhn, P.-G. Reinhard, P. D. Stevenson, and A. S. Umar, The TDHF code Sky3D, Comput. Phys. Commun. **185**, 2195 (2014).

[135] S. A. Umar and C. Simenel, TDHF investigations of the U+U quasifission process, Acta Phys. Pol. **49**, 573 (2018).

[136] S. Jin, K. J. Roche, A. Bulgac, and I. Stetcu, The SLDA code: A solver for static and time-dependent superfluid local density approximation (SLDA) equations in 3D coordinate space (unpublished).

[137] K.-H. Kim, T. Otsuka, and P. Bonche, Three-dimensional TDHF calculations for reactions of unstable nuclei, J. Phys. G: Nucl. Part. Phys. **23**, 1267 (1997).

[138] D. V. Schroeder, *An Introduction to Thermal Physcs* (Addison Wesley Longman, San Francisco, 1999).

[139] D. M. Brink, M. J. Giannoni, and M. Veneroni, Derivation of an adiabatic time-dependent Hartree-Fock formalism from a variational principle, Nucl. Phys. A **258**, 237 (1976).

[140] R. E. Peierls and D. J. Thouless, Variational approach to collective motion, Nucl. Phys. **38**, 154 (1962).

[141] R. Bernard, H. Goutte, D. Gogny, and W. Younes, Microscopic and nonadiabatic Schrödinger equation derived from the generator coordinate method based on zero- and two-quasiparticle states, Phys. Rev. C **84**, 044308 (2011).

[142] H. Uhrenholt, S. Åberg, A. Dobrowolski, T. Døssing, T. Ichikawa, and P. Möller, Combinatorial nuclear level-density model, Nucl. Phys. A **913**, 127 (2013).

[143] G. F. Bertsch and L. M. Robledo, Combinatorial level densities by the real-time method, Comput. Phys. Commun. **185**, 3406 (2014).